Development of a deployable arm to hold mirrors for space interferometric instrument

Auteur : Mansoor, Zain
Promoteur(s) : Bruls, Olivier; Loicq, Jerome
Faculté : Faculté des Sciences appliquées
Diplôme : Master en ingénieur civil mécanicien, à finalité spécialisée en génie mécanique
Année académique : 2017-2018
URI/URL : http://hdl.handle.net/2268.2/5447

University of Liège
Faculty of Applied Sciences

Development of a deployable arm to hold mirrors for space interferometric instrument

Author
Zain Mansoor

Supervisors
Olivier Brüls
Jerôme Loicq

Readers
Duysinx Pierre
Collette Christophe
Jacobs Jérôme

Thesis submitted in partial fulfilment of the requirements
for the Master's degree in Mechanical Engineering

Academic year 2017-2018

Abstract

This master thesis consists in the study of a deployable arm to provide a baseline for holding mirrors for a space based interferometer. High stability and accuracy is required to obtain a good quality imaging. The objective of the Centre Spatial de Liège is to develop an astronomical interferometer.

Firstly, a review of deployable technology is done in order to determine technologies that are currently available. It is followed by a classification of different structures. Secondly, the selection of a technology is performed. A preliminary design of some deployable structures is done and a static analysis and a modal analysis is performed. On the basis of this, the most appropriate technology for a small astrophysics mission is chosen. Thirdly, a pre-design of a deployable structure is carried out by using the selected technology. The static and modal analysis is done to evaluate improvements.

Finally, the deployable arm for a space based interferometer is feasible. However, some assumptions have to be verified.

Acknowledgements

First of all, I would like to express my gratitude to my supervisor Professor Olivier Brüls for giving me the opportunity to work on this subject, for his support throughout this work, his guidance and his advice.

I am also thankful to Prof. Jerôme Loicq and Jérôme Jacobs from CSL for their valuable help when I encountered difficulties.

Then, I would like to express my gratitude to Prof.Laurent Duchêne for helping me with some issues and for his availability and expertise.

I would like to thank Ms.Vaessen France and Coraline Gaspar for their help.

Finally, I would like to thank my friends, my family and in particular my parents for supporting me along this work.

Contents

List of Figures **6**

List of Tables **10**

1 Introduction **11**

2 State of the art **13**

2.1 Deployable structure applications 13

2.1.1 Solar panels 13

2.1.2 Deployable antennas 14

2.1.3 Deployable telescope 17

2.2 Different deployable structure technologies 19

2.2.1 Inflatable booms 19

2.2.2 Telescopic booms 20

2.2.3 CoilABLE boom 24

2.2.4 Articulated truss structure 24

2.2.5 Thin-walled deployable boom 26

2.2.6 Articulated boom 29

2.2.7 Conclusion 30

3 Problem definition and specification **31**

3.1 Space interferometry 31

3.2 Requirements and constraints 34

3.3 Specifications 36

4 Technology selection **38**

4.1 Analysis of the technologies 38

4.2 First pre-design 43

4.3 Static analysis of the selected technology 51

4.3.1 Load case 51

4.3.2 Telescopic boom 52

4.3.3 Articulated boom 56

4.3.4 Collapsible Tube Mast 57

4.4 Modal analysis 58

4.4.1 Modelling 58

4.4.2 Determination of $\mathbf{K_s}$ and $\mathbf{M_s}$ 59

4.4.3 Eigen frequencies 60

4.4.4 Results 61

4.5 Comparison 62

4.5.1 Static analysis results 62

4.5.2 Modal analysis results 65

4.5.3 Conclusion 67

5 Pre-design **68**

5.1 Configuration 68

5.2 Static analysis 70
5.2.1 Modal analysis 73
5.3 Conclusion 75

6 Further work **76**

7 Conclusion **78**

Appendices **80**

A Detailed static analysis developments **81**

B **84**

Bibliography **86**

List of Figures

2.1 Dawn deployed solar arrays [1] 14

2.2 Inflatable Solar array by NASA [2]. 14

2.3 AstroMesh reflector by Northrop Grumman Astro Aerospace for NASA JPL's SMAP [3]. 15

2.4 The deployed inflatable Antenna Experiment (IAE) by L'Garde NASA/JPL [4]. 16

2.5 Deployment sequence of the Solid Surface Deployable Antenna [5]. 16

2.6 The Picosatellite for Remote Sensing and innovative Space Missions (PRISM) [6]. 17

2.7 The James Webb Space Telescope (JWST) by NASA, ESA and ASC [7]. 18

2.8 The James Webb Space Telescope in the fairing envelope of Ariane 5 [7]. 19

2.9 Inflatable boom by NASA, in folded and unfolded configuration [8]. . . . 20

2.10 Telescopic boom actuated by spindle and nut [9]. 21

2.11 Telescopic boom actuated by cable and pulley [9]. 21

2.12 Telescopic boom actuated by a bi-STEM [10]. 22

2.13 AstroTube ^{TM} Max Telescopic Boom by Oxford Space Systems [11]. . . . 22

2.14 The Able Deployable Articulated Mast (ADAM) by NASA [12]. 23

2.15 Four longerons CoilABLE boom developed by ATK [13]. 24

2.16 The stowed configuration of the SPIRIT by NASA. 25

2.17 The deployment of the SPIRIT, rotation of the first hinge by 90°. 25

2.18 The deployment of the SPIRIT, rotation of the second hinge by 90°. . . 25

2.19 The deployment of the SPIRIT, rotation of the third hinge by 180°. . . 25

2.20 The deployment of the SPIRIT, rotation of the fourth hinge by 90°. . . 25

2.21 Complete deployment configuration of the SPIRIT, rotation of the fourth hinge by 180°. 25

2.22 The Bistable Tape Spring (BTS) [14]. 27

2.23 The Collapsible Tube Mast (CTM) [15]. 28

2.24 The Storable Tubular Extendible Member (STEM) [16]. 28

2.25 The Hubble Space Telescope solar array deployment system [17]. 28

2.26 The SpaceX Dragon Cargo hold by the Canadarm2 in the ISS [18]. . . . 30

2.27 The Articulated Deployment System from Airbus Defense and Space Netherlands [19]. 30

3.1 Airy pattern. 32

3.2 Airy pattern of the two closest objects when the lens aperture increases (from left to right). 32

3.3 Very Large Array (VLA) radio interferometer in Socorro Country, US [20]. 33

3.4 Very Large Telescope (VLT) operating in visible and infrared wavelenghts in Atacama Desert, Chile [21]. 33

3.5 Evolution of the mass of mirror in function of its diameter and the material used. 37

4.1 Boom diameter in function of the deployable length and the type of technology [22]. 39

4.2 Packaging ratio in function of the deployable length and the type of technology [22]. 40

4.3 Boom mass in function of the deployable length and the type of technology [22]. 42

4.4 Bending stiffness in function of the deployable length and the type of technology [22]. 43

4.5 Simplified model of the Telescopic boom. 44

4.6 Simplify model of the Articulated boom. 45

4.7 First quadrant of the lenticular cross-section of the Collapsible Tube Mast. 46

4.8 Lips of Collapsible Tube Mast. 46

4.9 Cross-section of radius R and angle α. 49

4.10 Simplified model of the Thin-walled deployable boom. 50

4.11 Smooth evolution of angle in function of the time. 51

4.12 Evolution of angular speed in function of the time. 51

4.13 Evolution of the angular acceleration in function of the time. 52

4.14 Free body diagrams of the fourth section of the boom. 54

4.15 Deflection of the Telescopic boom under an angular acceleration of 0.01 rad/s^2. 56

4.16 Deflection of the Articulated boom under an angular acceleration of 0.01 rad/s^2. 57

4.17 Deflection of the Collapsible boom under an angular acceleration of 0.01 rad/s^2. 58

4.18 The local axes of an element. 59

4.19 Occupied area in function of weight for the bending stiffness 2 10^4 N/m^2 of the y-axis of the Collapsible Tube Mast, the bending stiffness of the Articulated and the Telescopic boom. 64

4.20 Occupied area in function of weight for the bending stiffness 2 10^4 N/m^2 of the x-axis of the Collapsible Tube Mast, the bending stiffness of the Articulated and the Telescopic boom. 64

4.21 Occupied area in function of weight for the bending stiffness 10^5 N/m^2 of the y-axis of the Collapsible Tube Mast, the bending stiffness of the Articulated and the Telescopic boom. 65

4.22 Occupied area in function of stowed volume for a first resonance frequency of 10 Hz. 66

5.1 Positioning of the three Collapsible Tube Mast. 69

5.2 Orientation and placement of the three Collapsible Tube Masts. 69

5.3 Simplified model of the system in the y-z plane. 70

5.4 Simplified model of the platform in the x-y plane. 71

5.5 Boom radius in function of weight for the bending stiffness 10^5 N/m^2 of the y-axis of the Collapsible Tube Mast and of the Collapsible system. . . 73

5.6 Boom radius in function of weight for the bending stiffness 5 10^5 N/m^2 of the y-axis of the Collapsible Tube Mast and of the Collapsible system. 74

5.7 Discretization model of the Collapsible system. 74

5.8 Boom radius in function of weight for a resonance frequency of 10 Hz of the Collapsible Tube Mast and of the Collapsible system. 75

A.1 Free body diagrams of the third section of the boom. 81

A.2 Free body diagrams of the second section of the boom. 82

A.3 Free body diagrams of the first section of the boom. 83

List of Tables

3.1 Material properties of Aluminum 7050. 37

4.1 Eigen frequencies of the Telescopic boom, Articulated boom and Collapsible Tube Mast. 62

Chapter 1

Introduction

Since earliest times, humans are curious to know what is in the space. In order to increase the size of the observed object and its luminosity, the telescope has been created. Therefore, at the end of the sixteenth century, the first refracting telescope was built. Few years later, Galileo began to observe the sky with its own telescope. And at the end of the seventeenth century, Newton built the first reflecting telescope. Humans have continued to improve this device with the aim of increasing the quality of the observation and to observe further. The diameter is the most important characteristic of the telescope,larger the telescope, better the imaging properties and the magnifying power. This leads to the construction of telescopes with larger aperture with the restriction of the technology and the cost.

Since the second half of the last century, a large amount of telescopes have been sent in the outer space. One could ask, why did the latter are placed in space ? The ground-based observatories on Earth have two main drawbacks. First, the atmosphere acts like a filter, only a portion of electromagnetic spectrum can reach the ground. Moreover, the atmosphere is totally opaque for wavelengths lower than 100 nm and bigger than 10 m. While the outer space telescope have access to all range of wavelength, which is a great advantage. Secondly, the ground-based observatories are subjected to distortion of electromagnetic radiation, which decreases the angular resolution of the telescope. This can be reduced by using adaptive optics, but the outer space telescope by nature does not have this problem. That is why they are interesting.

However, to see further in the space, a high angular resolution is needed, which leads to telescopes with large aperture and long focal length.

Even if it is not easy to build a ground-based observatory with a large aperture, it is still possible by building mirrors with multiple segments, for example the Southern African Large Telescope (SALT). Nevertheless, it becomes much more complicated and

expensive to reproduce them in the outer space. One of the solution, which becomes more and more popular, is the astronomical interferometer. Theoretically, it gives an angular resolution equivalent of a telescope with an aperture equal to the distance between the telescopes which composes the astronomical interferometer.

The long term objective for the Centre Spatial de Liège is the development of an astronomical interferometer composed of at least two telescopes, which will allow the study of exo-planets. A second master thesis is being done in parallel by another student, his aim is to develop the pair of the telescopes.

Another task is the development of arms which will hold those two telescopes. The spacecraft fairing envelope, which will carry out the astrophysics observatory, directly limits the size of this latter. For example, Herschel telescope has 3.5 m aperture mirror, which is almost the maximum size of an Ariane 5 fairing envelope. One solution can be the development of larger launchers, which is not reasonable, given the cost of the development. Another solution is to use a deployable structure which will increase the baseline of the astronomical interferometer once in orbit, instead of using a large rigid structure.

This leads to the aim of this Master Thesis, the objective is to study the development of a deployable arm to hold telescope with high stability and high accuracy, which are primordial needs for interferometry instruments. A state of the art is performed in order to know what technologies are currently available and they are classified according to their deployment technique. Then, an introduction on the space interferometry will be done in order to understand the concept. Form there, the problem will be defined, the requirements are presented and the specification are determined. On the basis of external articles and reviews, a first selection is undertaken. After that, the selected structure are subjected to a preliminary design, which is used to perform the static analysis that is done analytically with *MATLAB*. Next, the modal analysis is done by finite elements in *MATLAB*. The results of these analyses lead to the selection of the most appropriate technology for a small astrophysics mission. The last section is devoted for the pre-design of a deployable structure based on the selected technology. A static and a modal analysis is carried out to evaluate the improvements.

Chapter 2

State of the art

This thesis aims to the study of an appropriate deployable technology for an astrophysics mission. These technologies have a rich history in the space field. First of all, a general review of the different deployable structures is developed. It starts with a look into the common applications for which these structures are used. Then, currently available technologies are presented and discussed.

2.1 Deployable structure applications

2.1.1 Solar panels

One of the most common applications of the deployable structure is the deployable solar panels. It allows the increase of the area of collection of the Sun power, as it is almost the only energy available in the outer-space and all the satellite functions are sized on it. A bigger power production enables to perform operations like sending a stronger signal to earth. Generally speaking, hinges are used to connect different solar panels between one another and it gives form to a "solar arrays wing". The unfolding of the solar arrays is carried out by using spring system. In addition, a locking system is also used to ensure the stability of the deployed configuration. Moreover, the solar arrays can have an orientation system to be sure that panels are always pointed to the sun and this way, increase the production power. Finally, there are some loads applied on the structure due to the vibration during the launch. By piling the solar panels on each other, the latter are protected from those loads. Figure 2.1 represents the space probe Dawn, designed by NASA, with the deployed solar arrays.

This is a classical way to put solar panels on a satellite. Some non-traditional ways are also being investigated including the inflatable solar array. Figure 2.2 shows the Inflatable Solar Array (ISA) developed by Marshall Center's Space Systems Department (NASA) and two industry partners, Jacobs Engineering and ManTech international. An inflatable structure is covered by a large number of solar cells. The folded structure takes up a small volume, like a small spacecraft. After some tests, the power produced in orbit around the earth, would be around 1 kilowatt, which is 100 times higher than the power produced by a traditional system for the same volume of packaging. Moreover, this system can be adapted for larger satellite missions or smaller cubesat missions and it can also be used for a rover or for deep space probe missions. The system is tested in laboratory environment and is considered to be at technology readiness level 4 on a scale of one to nine.

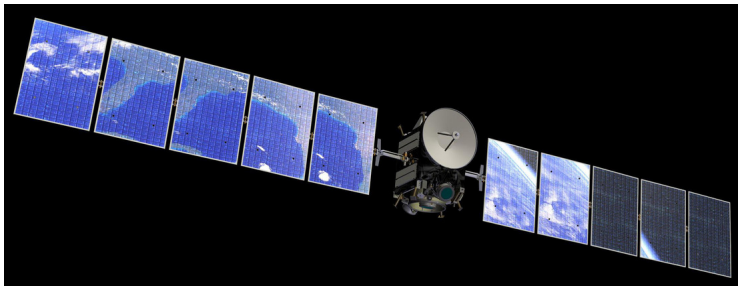

Figure 2.1: Dawn deployed solar arrays [1]

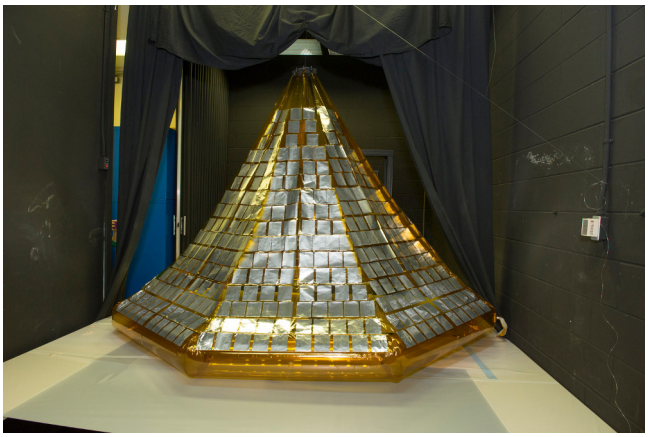

Figure 2.2: Inflatable Solar array by NASA [2].

2.1.2 Deployable antennas

The next application, in which deployable systems are widely used, is the deployable antennas. They are an essential part of a satellite, without them the satellite wouldn't

be able to receive any orders or transmit data, which is essential for the success of a mission. There are several types of deployable antennas such as Mesh antennas, inflatable antennas and solid surface antennas.

Firstly, Mesh antennas allow the use of antennas with great aperture, with a diameter which is lager than the fairing envelope one. The Larger the reflector, the higher the gain. Furthermore, it can be used as a multi-beam antenna and thus reduces the number of satellite used. Figure 2.3 illustrates the AstroMesh [3], it is designed and built by a Northrop Grumman Corporation company, Astro Aerospace. The latter is very lightweight, it has low stowed volume, low surface distortion and low cost compared to other Mesh reflectors. The AstroMesh is used aboard the Soil Moisture Active Passive satellite of which the mission consists in the global measurements of soil moisture.

Secondly, the inflatable antenna has the same advantages as the Mesh antenna with a ratio of compactness which is much higer, it is even more lightweight and an inexpensive structure. Compared to the Mesh antenna, there is no need for any mechanical actuators, thus the structure deployment is more reliable than other mechanical systems. Figure 2.4 shows the Inflatable Antenna Experiment [4] designed by L'Garde and NASA/JPL in the nineties.

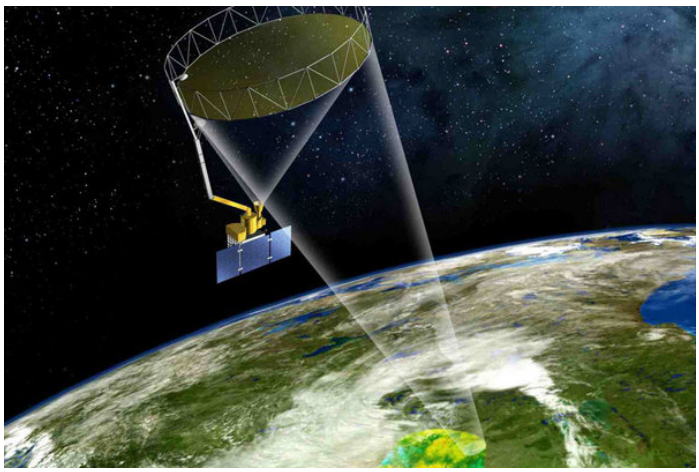

Figure 2.3: AstroMesh reflector by Northrop Grumman Astro Aerospace for NASA JPL's SMAP [3].

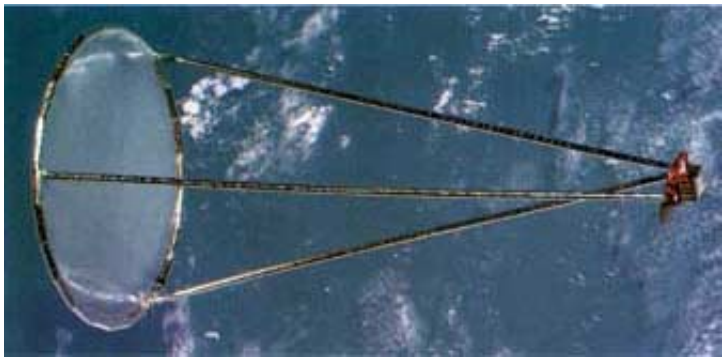

Figure 2.4: The deployed inflatable Antenna Experiment (IAE) by L'Garde NASA/JPL [4].

Thirdly, the solid surface antenna is another alternative antenna. This latter is very useful for high operating frequency which requires a solid reflective surface. Figure 2.5 displays the deployment sequence of the Solid Surface Deployable Antenna [5] designed by Simon Guest and Sergio Pellegrino. The SSDA is composed of several panels rolled around a hub, each panel is being deployed thanks to motors.

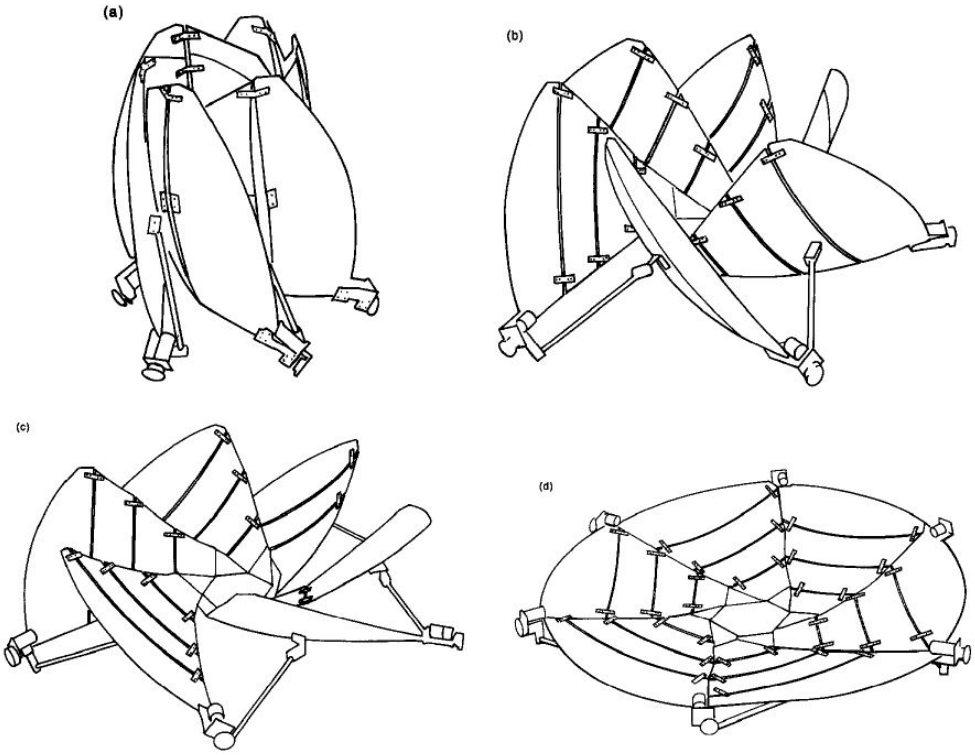

Figure 2.5: Deployment sequence of the Solid Surface Deployable Antenna [5].

2.1.3 Deployable telescope

The third application, and the last to be mentioned, for which the deployable systems are developed, is the deployable telescope. There are two principal features that can be improved with a deployable system : increase of the aperture and increase of the focal length.

Figure 2.6 illustrates the Picosatellite for Remote Sensing and Innovative Space Missions (PRISM) [6] developed by intelligent Space Systems Labatory at the University of Tokyo, with some other laboratory in Japan and with industries. The aim of the mission was to prove that a high/medium resolution imaging can be done with low cost mission. The satellite has a size of 20x20x40 cm^3 with a total mass of approximately 8 kg. The deployable structure enables a focal length of 50 cm which allows to have a ground resolution of 30 m per pixel from an orbital altitude of 800 km. The focal length is increased by attaching the lens at the tip of the extensible boom. The main task is the deployable structure which has to be accurately aligned and has to be stable under various perturbations of the space environment.

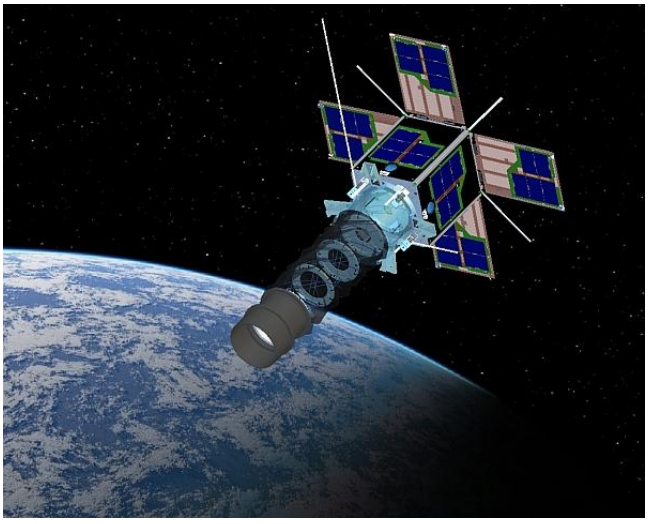

Figure 2.6: The Picosatellite for Remote Sensing and innovative Space Missions (PRISM) [6].

Another telescope that uses deployable structures is the JWST [23] (James Webb Space Telescope), illustrated in Figure 2.7, which is the successor to the well known HST (Hubble space telescope). The JWST is the most complex and the largest orbiting optical observatory ever built. Unlike the HST, the JWST is used to observe in the infrared region and its aim is to study, among others, the first stars, the first galaxies and the nature of the dark matter. This exceptional observatory is too big to enter the fairing envelope of any launcher available nowadays, the diameter of the primary mirror

is about 6,5 m. The solution is to build the telescope with deployable structures. One of the major challenge is the deployable system for the primary mirror, it is composed of 18 individual segments of beryllium mirros. The primary mirror is built to be folded by section, into 3 pieces, to be able to fit in the fairing envelope of the launcher Ariane 5, as it can be seen in Figure 2.8.

Given that the observations will be carried out in the near-infrared and mid-infrared wavebands, the observatory needs to be cooled at about 37 K in order to obtain a good performance. To achieve this, it is necessary to use a sunshield and to cool the entire telescope. Another major challenge is the deployable system for the multilayer sunshield, the latter will keep the telescope under shadow. Moreover, there is a secondary mirror which is placed away from the primary one. It is placed on an articulated tripod which is folded for the launch.

After the launch, the deployment sequence will start with the unfolding of the articulated tripod, then the primary mirror will take form and finally the large sunshield will be deployed in order to bring the thermal condition necessary for the good operating.

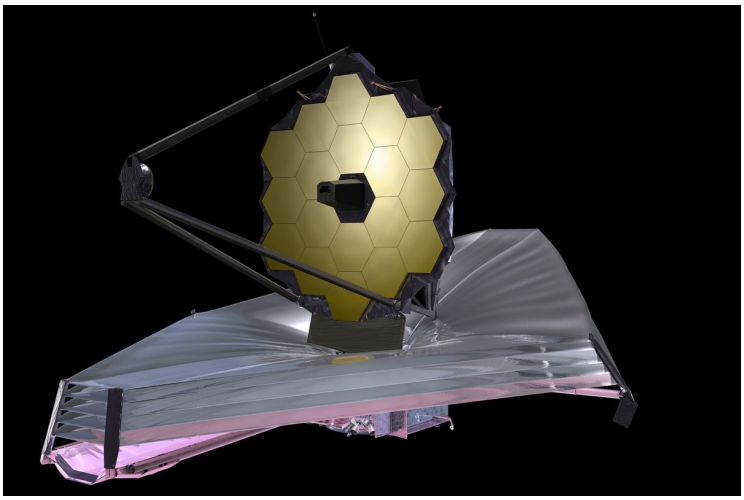

Figure 2.7: The James Webb Space Telescope (JWST) by NASA, ESA and ASC [7].

Figure 2.8: The James Webb Space Telescope in the fairing envelope of Ariane 5 [7].

2.2 Different deployable structure technologies

In the previous section, some main applications of the deployable system have been described in order to show their important role in a spacecraft. Indeed, without the latter it would not be possible to put into orbit bigger satellites than a fairing envelope. However, no single detail is given about their performances. In this section, the main technologies of deployable structures currently available are presented with their advantages and drawbacks. This is a non-exhaustive list.

2.2.1 Inflatable booms

Inflatable booms are tubes that take a very small volume in deflated mode, they are deployed by inflating gas in them. The deployment mechanism is very simple compared to other systems, hence they are very reliable systems. Figure 2.9 shows the inflatable boom, on the left side the folded configuration and on the other side the unfolded configuration. The space environment is very harsh, micro-meteorites or space debris can damage the boom, which can lead to outgassing and depressurisation. Therefore, it is interesting to harden the inflatable structure after it has achieved its final shape. There

are many possibilities of rigidization process [24] as UV setting resins, thermosetting resins, glass transition resins or embedded structural components etc.

The UV setting resin gives a low outgassing and long storage life. It can be used for wide range of structure shapes. The curring can be done by using the sun radiation which is called passive rigidization process or by using embedded lamps in order to control the cure but it will lead to a more complex system. Moreover, in the latter case, the premature rigidization has to be avoided by controlling the covering of the structure from the sun radiation.

On one hand this category of deployable structure has some interesting advantages such as being a very lightweight structure, having an extremely high packaging ratio, and a simple deployment system which gives a highly reliable structure. On the other hand, it has a low deployment accuracy, from a few millimetres to several centimetres. It also has a low stability after deployment and a very small load bearing capacity, which makes it, at first sight, inadequate for application requiring precision.

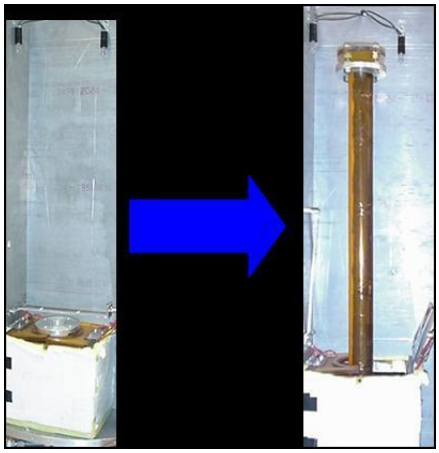

Figure 2.9: Inflatable boom by NASA, in folded and unfolded configuration [8].

2.2.2 Telescopic booms

Telescopic booms are a series of tubes that are interlocked into each other and at each progressive stage the diameter of the tube becomes smaller, which leads to a very compact system. When deployed, one tube slides out from the other either sequentially or symmetrically. The interlocked tubes can be built with metallic or composite materials. Moreover, they have a good resistance to failure against micro-meteorites or space debris. In fact the impact of micro-meteorites on the structure usually causes perforations. Nevertheless the system is still operational for a small number of impacts and if the interconnection are unharmed.

The deployment mechanism is more elaborate than the previous technology, which leads to a system that is a little bit more complex, thus there is more risk of failure in this technology which makes it less reliable than the Inflatable booms. There are different possibilities for deployment as an inflatable boom configuration, the spindle and nut configuration, cable and pulley configuration, bi-STEM configuration. Figure 2.10, 2.11 and 2.12 illustrate respectively the last three configurations.

The main challenge with this technology is to obtain a good stiffness, the overlapping of the adjacent tubes increases it. If there are surface irregularities or the tubes thickness is too small, a larger overlap between tubes is needed. On one hand the greater the overlap, the stiffer the system but on the other hand the maximum deployable length decreases and the deployable nonstructural weight increases, consequently there is a trade-off. Furthermore, the design should take into account the risk of jam due to the elastic or thermal deformation at the overlapping level.

Latches design are also very important as they are crucial parts of the system, the structural efficiency and reliability will depend mainly on them. The latter are inserted between the tubular segments in order to wedge the tubes once fully deployed. Unfortunately, there is always a play between the latch and the tubes, the design should try to minimise it.

This deployable technology has plenty of advantages, it is much stiffer than other systems, it has a good positioning precision from a few micrometres to several millimetres. It also has a good stability after deployment, a very small stowed length and depending on the material used and the tubes thickness it could undergo heavy load. Nonetheless, the structure is heavy, it has a low packaging ratio and the deployment mechanism is complex, as discussed above.

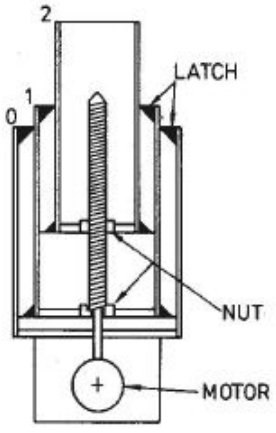

Figure 2.10: Telescopic boom actuated by spindle and nut [9].

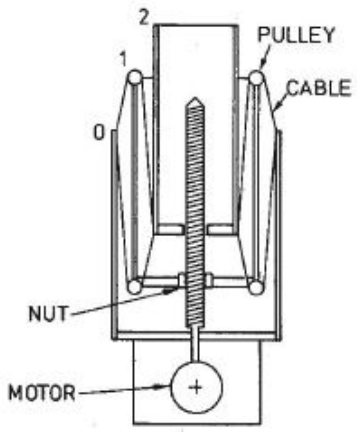

Figure 2.11: Telescopic boom actuated by cable and pulley [9].

Figure 2.13 represents the AstroTube ^{TM} Max Telescopic Boom developed by Oxford Space Systems [11]. It is a telescopic boom which is scaleable for different types of missions, from 0.5 m to 15m with a one shot deployment or a retractable system. The system is deployed by two Storable Tubular Extendable Member called bi-STEM mechanism.

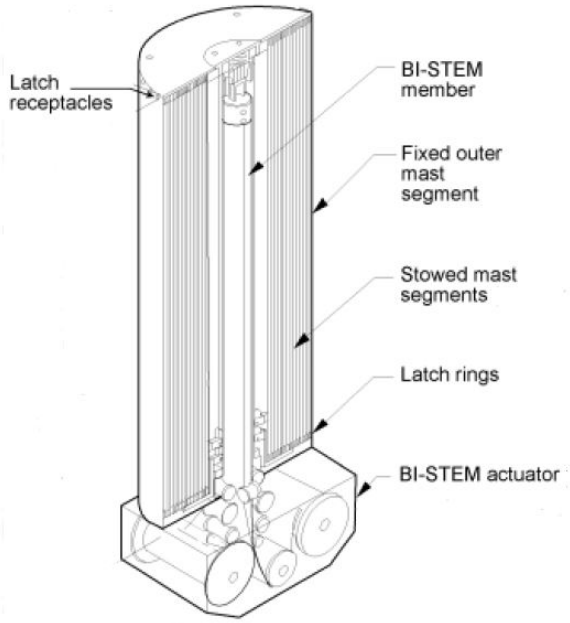

Figure 2.12: Telescopic boom actuated by a bi-STEM [10].

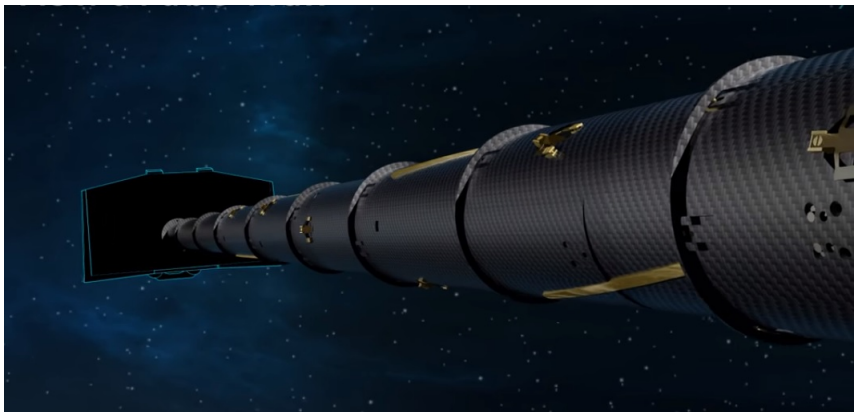

Figure 2.13: AstroTube ^{TM} Max Telescopic Boom by Oxford Space Systems [11].

Deployable truss structure

This technology is a truss-like structure, it is composed of several longerons connected to one another by pinned joints in order to store and deploy the structure. The tensegrity structure comes in this category, the principle is that isolated longerons are compressed to each others by a prestressed tensioned net. Figure 2.14 illustrates the ADAM mast developed by NASA and built by the AEC-Able Engineering Company, Inc. ADAM mast is flight proven and was used for NASA Shuttle Radar Topography Mission, the extension is about 60 m. In order to stiffen the structure, diagonal cables are used as latch at each module level, once deployed.

Figure 2.14: The Able Deployable Articulated Mast (ADAM) by NASA [12].

The main advantages are as follows. Firstly, an extremely compact storage volume, in the case of ADAM the storage length is about 5% of the deployable length. Secondly, the structure allows the creation of deployable masts extending to some tens of metres, 60 meters for ADAM Mast. Thirdly, it is a lightweight structure with a mass of approximately 360 kg. Finally, the diameter and the length of the longerons can be selected to undergo a given load. However, this structure has a coarse positioning, from a few millimetres to several centimetres. It has also a very low stability after deployment, indeed there is a length variation of about 10 mm due to thermal distortion and a bending of about 0.1°.

2.2.3 CoilABLE boom

The CoilABLE boom technology is based on the elastic deformation energy. It consists of longerons, battens and diagonals. Battens are components which are perpendicular to the longerons. In the folded configuration, the longerons are coiled which gives the strain energy used for the deployment. Unlike the longerons of the deployable truss structure, the longerons in the CoilABLE are not isolated parts but the full length of longerons are deformed, acting like a spring. Furthermore, during the deployment the tip rotates. Like ADAM, this type of boom has also a long inheritance and thus is flight proven. Figure 2.15 shows the ATK's CoilABLE boom with carbon fiber longerons [22]. In the previous section, PRISM satellite is described. The latter also uses a CoilABLE boom to increase the focal length.

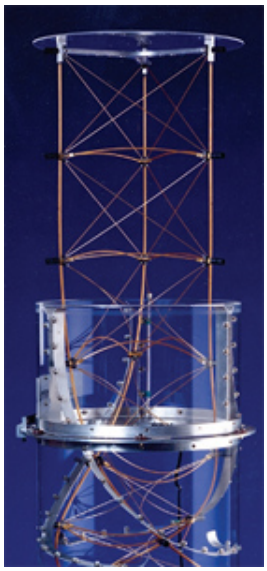

Figure 2.15: Four longerons CoilABLE boom developed by ATK [13].

This technology is even more lightweight and more compact than the Deployable truss structure. Indeed the stowed length is less than 2% of the deployed length. However, like the latter, it has a low stability after positioning and a low accurate positioning, from some millimetres up to several centimetres.

2.2.4 Articulated truss structure

The articulated truss structure is a rigid lattice structure that can be folded by inserting hinges. The system could either be a one shot deployment or a controlled deployment

with retraction that can be considered with a cable system or by controlling the hinges with motors. The structure performance depends on the stiffness of the hinges.

One example of space application is the SPIRIT (Space Infrared Interferometric Telescope) developed by NASA [25], Figure 2.16 and 2.21 illustrate respectively the stowed configuration and the fully deployed configuration of SPIRIT. The objectives are to study the formation of planetary systems, to characterize the family of extrasolar planetary and to learn the setting up of high-redshift galaxies and their merging into the present galaxies.

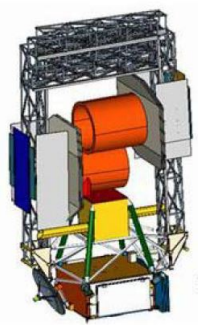

Figure 2.16: The stowed configuration of the SPIRIT by NASA.

Figure 2.17: The deployment of the SPIRIT, rotation of the first hinge by 90°.

Figure 2.18: The deployment of the SPIRIT, rotation of the second hinge by 90°.

Figure 2.19: The deployment of the SPIRIT, rotation of the third hinge by 180°.

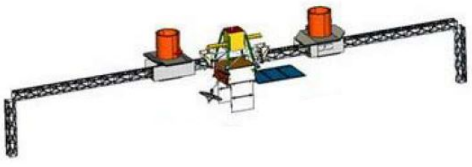

Figure 2.20: The deployment of the SPIRIT, rotation of the fourth hinge by 90°.

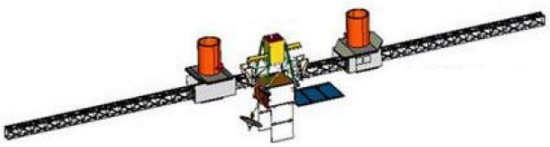

Figure 2.21: Complete deployment configuration of the SPIRIT, rotation of the fourth hinge by 180°.

The SPIRIT observatory uses a 36 m long rigid truss structure divided in two parts and attached to the central module, called the Instrument Module Assembly (IMA). Afocal Collector Telescopes (ACT) are placed on the rails of the both truss structures, as it can be seen in Figure 2.21. The ACT can move along the booms allowing a baseline from 6 m to 36 m, the former consists of a cryogenic telescope system with an aperture of 1 m, a combiner optics and a metrology optics.

It is envisaged to put this observatory into the L2 orbit. Once into this orbit, the SPIRIT will start the deployment sequence represented from Figure 2.16 to Figure 2.21. Moreover, in order to stabilise the structure once deployed, latches are used. Due to the overall cost, the mission is held until further notice.

This technology is well suited for applications that need high stiffness and very good post-deployment stability. It has also quite good positioning. However, it is a considerably heavy structure with a complex mechanism for the telescope's movement. Moreover, this technology has a very low packaging ratio.

2.2.5 Thin-walled deployable boom

The Thin-walled deployable boom is a structure that can be flattened and rolled up around a drum, the latter is deployed elastically from its stowed configuration to a boom configuration. Commonly, a thin structure has a low stiffness in compression for axial force and in bending for the transverse force. Nonetheless, it is surmounted by the profile of the structure which increases the area moment and thus the stiffness of the boom. There are different types of profile including the Bistable Tape Spring (BTS), the Collapsible Tube Mast (CTM), the Storable Tubular Extendable Member (STEM). These structures are generally made with stainless steel or the Carbon Fiber Reinforced Plastic Composites (CFRP).

Firstly, the BTS is illustrated in Figure 2.22, the cross-section of this boom is a circular arc. The latter is stable in both the stow and the deployable configuration, unlike STEM or CTM there is no mechanism needed to keep the system in these two configurations. Moreover, BTS need less strain to flatten, which reduces the size of the flatten system. This type of Thin-walled deployable boom is very compact with a simple mechanism for the winding and deployment.

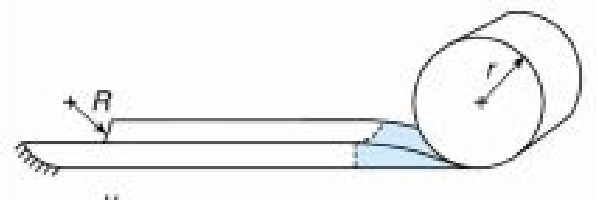

Figure 2.22: The Bistable Tape Spring (BTS) [14].

Secondly, the CTM is composed of two strips that are bonded together along the two edges by glueing or welding depending on the strip material. The cross-section has a lenticular profile, the shape gives the best torsional stiffness compared to the other two shapes.

Thirdly, the STEM has a cross-section which makes an open circle with an overlap, thus the area moment increases and intrinsically the stiffness in bending and in compression rise. However, there is a low torsion stiffness and it will mainly depend on the friction in the overlap region. A Variant of the STEM is the Bi-STEM which consists in using two diametrically opposed strips. The latter gives better properties with an increase in the bending and torsional stiffness, Whereas there is a small increase in the weight and the packaging volume. Another variant is the Interlocking Bi-STEM, the inner STEM has interlocking tabs along the edge and the latter are set in the matching holes of the outer STEM, in the deployment state. This configuration improves the torsional stiffness by locking the strips between together. Figure 2.24 illustrates the STEM with its variants.

The STEM is space qualified. Indeed, they are being used as actuators, for example in the $AstroTube^{TM}$ Max Telescopic boom. Moreover, it has also been used and is still used as booms in a large number of space missions, for example in the Hubble space telescope, the solar arrays are deployed thanks to a Bi-STEM boom, a representation is shown in Figure 2.25.

Such technology is very useful for space applications, as it has a very good packaging ratio and it is very lightweight. However, the bending and compression stiffness is not the best, but it can be enhanced by improving the cross-section, the deployment mechanism and the strip material. This technology has a lot of potential and, as a result, studies are ongoing in order to obtain better performances.

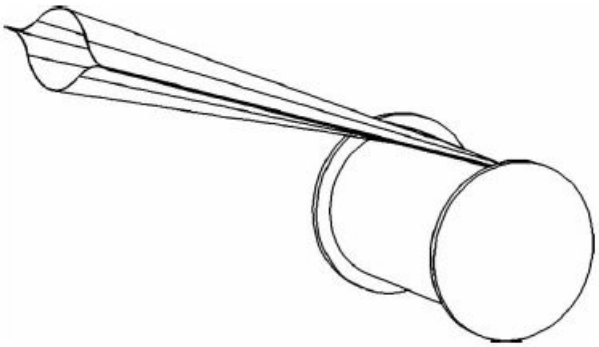

Figure 2.23: The Collapsible Tube Mast (CTM) [15].

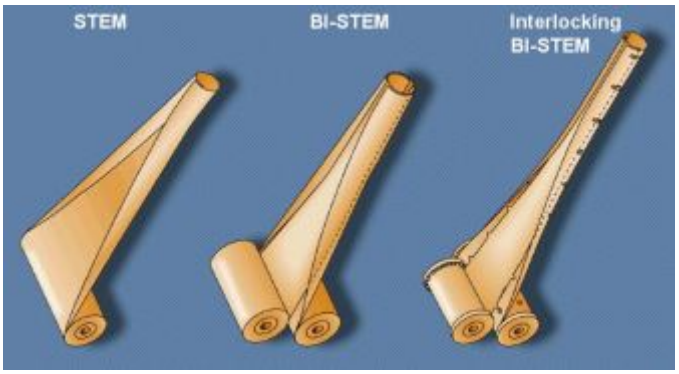

Figure 2.24: The Storable Tubular Extendible Member (STEM) [16].

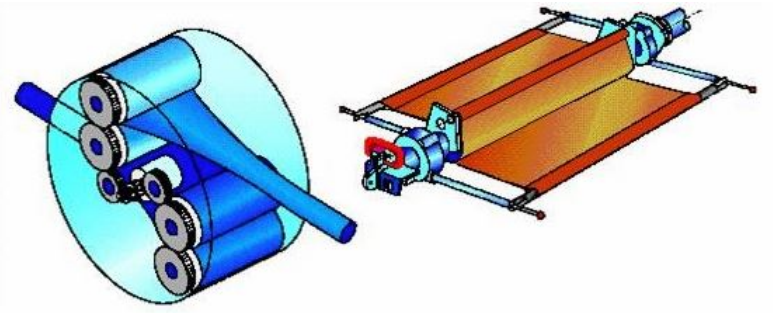

Figure 2.25: The Hubble Space Telescope solar array deployment system [17].

2.2.6 Articulated boom

The Articulated boom is a structure composed of several rigid parts with adjacent parts connected together with one or several joints. This is a kind of robotic arm. This technology can give 6 degrees of freedom in the space while the other ones only give 1 or 2 degrees of freedom at the most. Therefore, the latter is well suited for complex manipulations as well as for a long-reach grasping, spacecraft berthing operations, satellites repairing or servicing operations, space assembling operation, positioning operation etc. The motion of the system can be considered by placing motors at the different hinges or by using cables.

One of the well-known articulated arms in the space field is the International Space Station robotic arm also called Canadarm2 [26]. When fully extended it is 17.6 meter long with a selfweight of 116 kilograms. It has 7 degrees of freedom and all the joints are motorised. This arm has force sensors, cameras etc. Each end of the arm are similar and allows the arm to grasp objects or to grip it to the International Space Station (ISS). The latter is built by MD Robotics of Brampton. Figure 2.26 shows the Canadarm2 grasping the SpaceX Dragon cargo spaceship from the ISS.

Another application is the Articulated Deployment Systems (ADS) developed by Airbus Defence and Space Netherlands [19]. The latter can be used for multi-axis deployment form 1.5 to 4 m depending on the configuration of the boom and for a mass lower than 30 kg. This boom can be tuned for a given mission by changing a few design parameters, the main elements used for this technology have a great flight inheritance. Indeed they have been used in more than 500 space deployments with a 100 percent of success. Figure 2.27 gives a representation of the ADS.

This technology has one of the best stiffnesses among all the technologies described. Like the Telescopic boom, the Articulated one has a very good deployment accuracy from a few micrometres to several millimiters. However, this technology represents a higher level of complexity, as the boom is often used for multi-axis motions, an algorithm is needed to drive the different actuators in order to reach the target points.

Figure 2.26: The SpaceX Dragon Cargo hold by the Canadarm2 in the ISS [18].

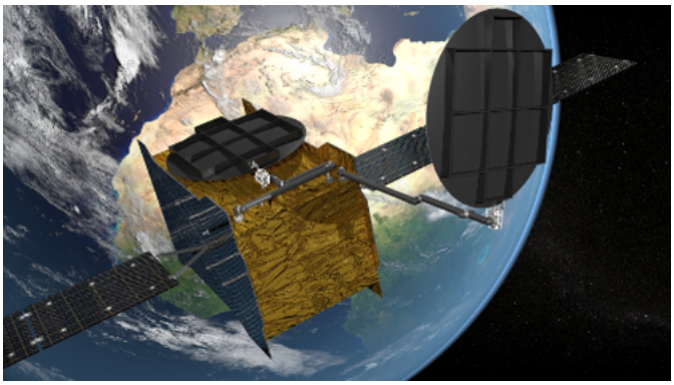

Figure 2.27: The Articulated Deployment System from Airbus Defense and Space Netherlands [19].

2.2.7 Conclusion

This overview allows to visualise the numerous applications in which deployable structures are used. Moreover, a large number of studies have been carried out in the space field on these structures for decades which is reflected by the several types of different technologies present in this section. Indeed, these technologies allow two main contributions. First, they enable to increase the performances of applications such as the enhancement of the electric power production by increasing the collecting area of solar panels. Then, they allow to reduce the cost of missions by decreasing the size and the weight of the satellite. These technologies will be subjected to a deep analysis in the following chapters.

Chapter 3

Problem definition and specification

Before analysing of the technologies, it is essential to define the problem and thus to determine the constraints. First, an introduction of the interferometry is done with the aim of understanding the concept in order to determine the constraints and requirements needed. Then, the specifications of the deployable arm related to the mission are presented.

3.1 Space interferometry

When light passes through an aperture, for example lenses or mirrors, it always causes diffraction. The image of a point is not a dot but a small bright circular zone surrounded alternatively by dark rings and bright rings, the further the bright ring is from the centre, the less brilliant it is. This is called Airy pattern, the central disk is the Airy disk which is illustrated in Figure 3.1. The size of the Airy disk is related to the angular resolution. Indeed the angular resolution is the smallest angle that can be distinguished between two closely placed objects. Therefore it is the angle between the centre of the bright disk and the first dark circle. The angular resolution for a circular aperture and if the light is only limited by diffration is given by :

$$\theta = 1.220\frac{\lambda}{D} \tag{3.1}$$

where θ is the angular resolution, λ the wavelength of the light and D is the diameter of the lens aperture. The largest separation distance between telescopes in the case of interferometry.

When the diameter D increases, the diameter of the Airy disk decreases and the angular resolution increases. The figure 3.2 shows the Airy pattern of the two closest objects. The left picture illustrates the image with a narrow circular aperture, when the diameter of this aperture is increased this gives a blurred image with two overlapped Airy disks (middle picture), in this case the two objects are unresolved. Finally, by increasing the diameter further, it is possible to distinguish the two objects, which are then resolved (right picture).

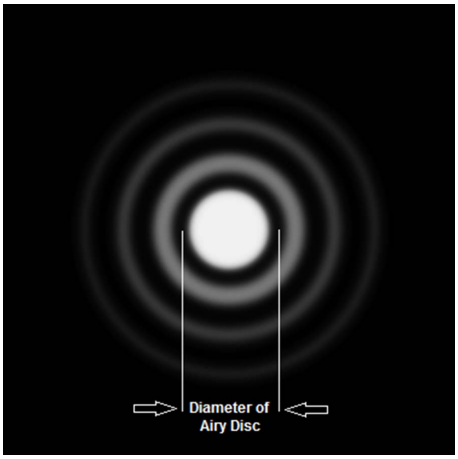

Figure 3.1: Airy pattern.

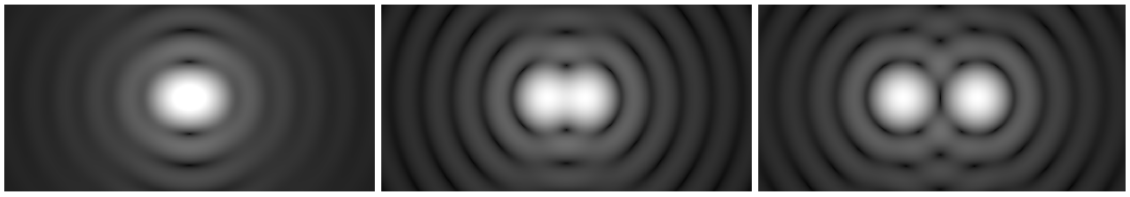

Figure 3.2: Airy pattern of the two closest objects when the lens aperture increases (from left to right).

Consequently, larger and larger telescopes are being built, with multiple segments, in order to have a better imaging quality and to see further in the space as the Giant Mahellan Telescope (GMT) with an angular resolution of a telescope of 24.5 m in diameter, scheduled for 2022. Moreover, the world's largest telescope under construction is the Extremely Large Telescope (ELT) with a segmented primary mirror of 39.3 meters.

An alternative to increase the angular resolution is by using the astronomical interferometer. It consists of using several separate telescopes, the light from these different telescopes is combined as if it was a single large telescope. This gives the angular

resolution for the largest separation between the telescopes. Nevertheless, it does not give the collecting area of the corresponding single telescope. However, this technique requires a coherent combination of waves, this means a constant phase difference between the wave source.

The interferometry is already being used with radio wavelength, wavelength up to 30 cm, for example the Very Large Array (VLA) represented in Figure 3.3. The latter is an observatory of 27 radio antennas arranged in a Y-shaped configuration. Each antenna is 25 m in diameter and the greatest angular resolution that can be reached is about 0.04 arcsecond, which is equivalent to a single antenna of 36 km in diameter. The control of the phase difference in radio waves is quite easy and the interferometry in radio waves has been used for decades.

Figure 3.3: Very Large Array (VLA) radio interferometer in Socorro Country, US [20].

Figure 3.4: Very Large Telescope (VLT) operating in visible and infrared wavelenghts in Atacama Desert, Chile [21].

Nevertheless, interferometry with optical waves is a much more challenging technique as the waves must be collected within a fraction of the light wavelength (between 700nm and 400nm), which requires an extremely accurate system. The Very Large Telescope (VLT) allows to do interferometry in the optical waves [27]. The VLT is composed of 4 fixed 8.2 m unit telescopes and the four movable 1.8m Auxiliary Telescopes illustrated in Figure 3.4. When all the telescopes are used together, they can achieve an angular resolution of about 0.001 arc-second.

The space based observatory has some serious advantages, explained above, that's why it is interesting to develop it. Space interferometer with a baseline under the size of a fairing envelope has already been studied (SIM), but, due to a lack of budget the mission was closed down by the end of 2010. Currently, there is no space based observatory sent for interferometry in the optical waves.

3.2 Requirements and constraints

The aim of this thesis is the development of an extension mechanism for a deployable baseline interferometer. The latter is composed of at least two deployable structures of similar length located opposite from each other with the satellite at the centre. In this subsection, the different requirements for a good extension mechanism and the constraints related to the mission are listed.

Deployment accuracy

It is one of the most important requirements to be fulfilled in order to obtain a good quality imaging. The desired accuracy depends on the wavelength in which the telescope will be operated. The supplementary thesis, on the development of the pair of telescopes is being conducted. Therefore, the exact wavelength is not available, the telescope will operate between the visible light and the Far infrared. The most constraining one is the Visible light. Indeed, the latter has a wave length between 380 nm (blue light) and 750 nm (red light), while far infrared is about a hundred micrometers. Accordingly, the deployment accuracy is a fraction of 380 nm and the latter is fixed to 40 nm. Yet, this accuracy is difficult to achieve with a boom or mast, some additional control systems will be necessary such as a second stage of active structure or a delay line often used in optic fields. The latter is discussed in the last chapter.

Post-deployment accuracy

This is also a very important requirement, space structures are subjected to different perturbations depending on where the spacecraft is located. The assumption of an observatory in orbit around the Earth is taken. In the latter case, the extension mechanism is subjected to vibrations due to perturbations coming from the spacecraft, for example vibrations of the flying wheels, or from the environment, for example the thermal effects due to solar radiation or the space debris. The accuracy has to be of the same order of magnitude as the deployment accuracy. Nevertheless, as there will be at least two extension mechanisms, the two opposite booms can vibrate if and only if they are in phase and with the same amplitude.

Eigen frequencies

In a static-load case, the greater the applied load, the larger the displacement/deformation, therefore the solution is to increase the stiffness of the structure. In dynamic load cases, the applied load magnitude is not as important as the frequency at which it is applied. Indeed, if a load of a certain magnitude is applied near the natural frequency of the structure, the response could be much larger than if the same load is applied at another frequency. Therefore, the first eigen frequency of the system should be as high as possible.

Volume of the system

This space mission is studied to build a space interferometer with a platform size of PROBA type. The latter is a name of the series of Belgian small satellites starting with PROBA-1, PROBA-2 and PROBA-V. Another satellite, PROBA-3, is planned with the objective to demonstrate the formation flying of multiple spacecrafts. The PROBA-V platform has a size of 75.6 x 73 x 84 cm, given that the volume taken by the telescopes and the other systems is not known yet, it is preferable to choose a deployable technology with a minimum volume in the stowed configuration.

Weight of the system

The weight of the payload has a significant impact on the cost of a mission. Indeed, the launch price of a spacecraft depends on the payload mass, size, orbit parameters and the launcher. For instance, one of the cheapest launchers is the Falcon 9 (a SpaceX launch vehicle). In fact, the cost for a launch is about \$60 to \$50 millon and the latter can lift a payload of up to 22,800 kg in Low Earth Orbit (LEO), which represents $\$2,632$

to $2,193 per kilogram. This is a medium-lift launch vehicle. There are also small-lift launch vehicles for small missions as Vega, developed by the Italian Space Agency and the European Space Agency, it can lift a payloads of up to 1500 kg in LEO for a cost of $37 million, which represents approximately $24,700 per kilogram. The weight of PROBA-V mission was about 140 kg, the space interferometer weight should be close to the latter. To sum up, the cost of the transportation represents 25% to 70 % of a space mission [28], therefore the weight is an important factor in the choice of the deployable technology.

3.3 Specifications

Length of the deployable mechanism

The first specification is related to the length of the deployable mechanism, this length depends on how far the observed target is placed. Indeed, this mission is limited to observe Alpha Centauri, which is the closest star system, about 4.37 light-years from the Sun. The size of the mechanism is estimated from 1 to 3 metres and for this study a length of 2 metres is taken as reference.

Payload mass

Secondly, the mass of the payload is an unknown variable. Nevertheless, it is important to use a realistic value for the technology analysis. There are four main types of material used to make mirrors such as Zerodur, Silicon carbide, Aluminum 6061 T6 and the Beryllium. Commonly, the mirrors are subjected to a lightened process. Indeed, the Hale telescope is 5m in diameter, after the mirror was hollowed out in honeycombs, it has lost 20 tons from its initial 40-ton mass. The percentage of hollowness depends on the properties of the material, in fact Zerodur, Silicon carbide, Aluminum 6061 T6 and Beryllium have alleviations of respectively 70%, 85%, 70% and 90%.

Figure 3.5 illustrates the mass of the primary mirror, depending on the diameter for the four different materials. This figure gives the order of magnitude of the weight. Among these materials, Beryllium is the lightest and the most expensive. Nevertheless, the latter is considered to be toxic. That is why it is not used, except in the USA. Whereas, Aluminum is the cheapest material, the easiest one to process and it has already been used for PROBA-V, therefore it will be used as a point of reference. The telescopes can be composed of several mirrors, the primary is the biggest one and it is assumed to be between 10 cm and 50 cm for a small mission as the future interferometer. The size of 30 cm is taken as an arbitrary choice, which gives a weight of 3.5 kg and in order to take the frame and other components of the telescope into account, the mass

is rounded up to 5 kg.

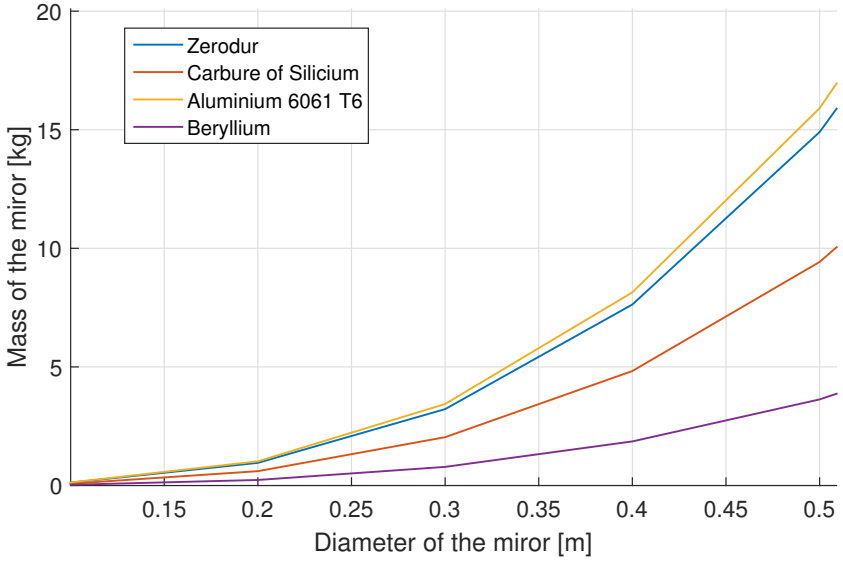

Figure 3.5: Evolution of the mass of mirror in function of its diameter and the material used.

Booms Material

Thirdly, it is necessary to define the material used for booms as properties like the Young's Modulus E, the density ρ are needed for the analysis. Composite materials are increasingly used in the space field. Indeed, the main quality is a significant mass saving. Moreover, the composite materials gives a very good stiffness and they can be tuned for a coefficient of thermal expansion near to zero. However, in this work the best material for the deployment mechanism is not studied and in order to simplify the analysis, a metallic material is chosen. Aluminum alloys are lightweight with good mechanical properties, they are often used in space field, the Aluminium 7050 is chosen arbitrarily as it can be used for Aerospace structures. Table 3.1 shows the Aluminum 7050 material properties.

Density ρ	Young's Modulus E	Thermal conductivity	Yield strength
2830 kg/m^3	71.5 GPa	130 $Wm/m^2°C$	400 MPa

Table 3.1: Material properties of Aluminum 7050.

Chapter 4

Technology selection

Now that the requirements and the constraints are known, the different systems can be compared. Firstly, technologies are compared through data available in the literature and a first selection is made on this basis. Secondly, the selected technologies will be subjected to a deep analysis and the one that fulfills the requirements the best is chosen.

4.1 Analysis of the technologies

Figures 4.1, 4.3 and 4.2 are taken from a review on deployable structure written by L. Puig, A. Barton and N. Rando [22]. This article gives valuable information, which is gathered in these figures. The latter are established on the basis of different technology analyses and testing. The points on the figure represent results of the different technologies, some of them are even flight proven. In addition, the results are extrapolated from data available in literature. The technologies are represented by different colours, as following :

- Dark blue : Inflatable booms
- Yellow : Telescopic booms
- Green : CoilABLE booms
- Light blue : Deployable truss structures
- Purple : Shape memory composite booms
- Red : Articulated booms

Firstly, Figure 4.1 shows the bulk of a boom depending on the length, the maximum diameter is also limited by the size of the PROBA-V platform. Secondly, Figure 4.3 illustrates the boom mass in function of the length. This is a very useful graph, at first glance, it can be observed that some technologies are too heavy for this mission. Then, there is Figure4.2 illustrating the packaging ratio, the latter is the ratio between the deployable length and the stowed length, with the diameter expressed in figure 4.1. It is possible to estimate the volume taken up by a given structure in the stowed and deployable configuration. Finally, Figure 4.4 illustrates the bending stiffness, booms generally have weaker stiffness in bending than in torsion or in axial direction. Therefore the main deformation will come from bending. For this reason the focus is on the bending stiffness and the others are not shown.

Concerning Articulated truss structure, the latter provides one of the best stiffness. The stiffness has a direct impact on the deployment accuracy, indeed the stiffer the structure is, the less deformed it is under loading. For this reason, this technology is well suited for astrophysics missions which is reflected by the study of the SPIRIT mission. However, this structure is one of the heavierst and in terms of volume it is the bulkiest. As a result, this technology is removed from the selection.

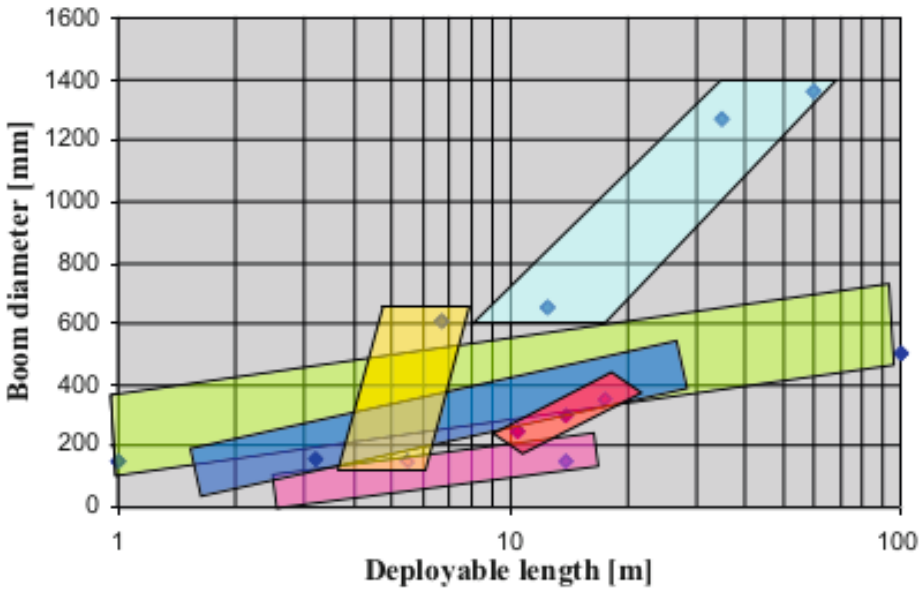

Figure 4.1: Boom diameter in function of the deployable length and the type of technology [22].

Then there is the Deployable Truss Structure, this technology has a significant flight legacy. It is often used for large length deployment such as a 8-meter boom for the advanced laboratory for communications and astronomy (HALCA) mission or a 60-

metre structure for ADAM mast, as presented in the previous chapter. It has a very good bending stiffness as seen in Figure 4.4. However, it is known to have a very coarse displacement in the axial and lateral directions. Moreover, this type of structure has a highly low fundamental frequency, about 0.1 Hz for ADAM mast [22] which often leads to a poor post-deployment accuracy. Therefore, this technology is not recommended for astrophysics applications.

After that, there is CoilABLE boom. It has a very lightweight structure. In fact, this technology allows to build a 100-meter boom with a weight between 20 and 4 kilograms, depending on the longerons properties. Moreover, this is an extremely compact structure, as it can be seen in Figure 4.2, the packaging ratio is about 0.04 and 0.03, while the diameter of the boom is approximately of 0.2 m and 0.4 m for respectively 1 and 3-meter boom length. For instance, it can be interesting to compute the stowed volume, which is given by :

$$V_{stowed} = \frac{\pi.D^2.L_{stowed}}{4} \tag{4.1}$$

where D is the diameter of the boom and L_{stowed} is the length of the boom in the stowed configuration.

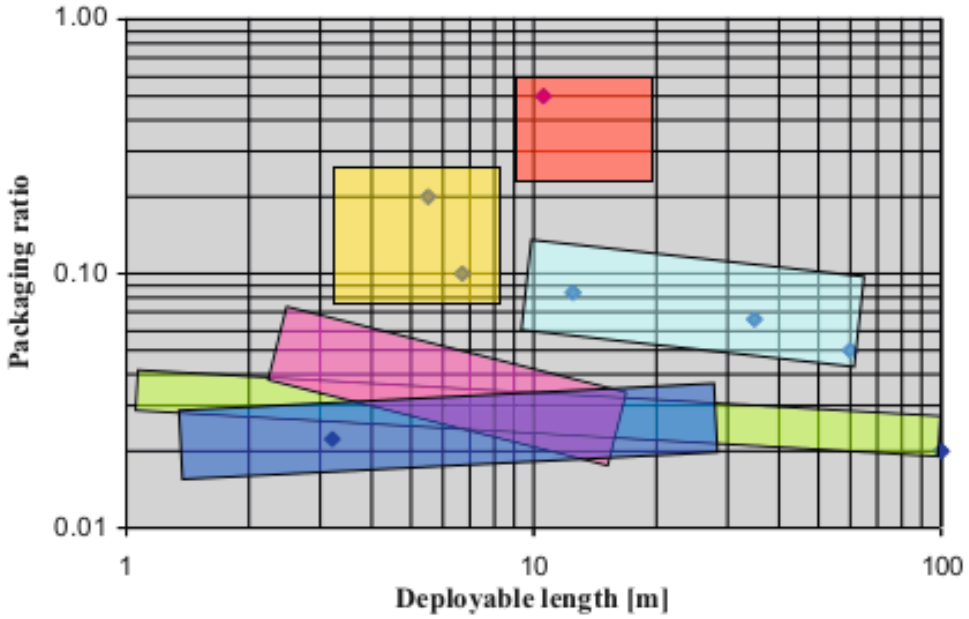

Figure 4.2: Packaging ratio in function of the deployable length and the type of technology [22].

The stowed volume is about 1.3 10^{-3} m^3 for a 1-meter length and about 1.13 10^{-2} m^3 for a 3-meter length, which represents respectively 0.27% and 2.4% of the

PROBA's platform volume. Even though this technology has a high range of bending stiffness as there is plenty of flexibility in the design of the longerons, it is not possible to achieve good stiffness without losing the coilAble property. Figure 4.4 shows the bending stiffness with an upper limit of 10^5 $N.m^2$. Moreover, stiffer longerons will take much more space in the stowed configuration. Thus, there is a trade-off to make. Like the Deployable truss structure, this one also has a considerable flight inheritance with applications requiring low deployment accuracy and low post-deployment stability, such as solar arrays. Actually, this structure is intrinsically not precise and stable but it also has low stiffness. As a consequence, the latter is not adequate for astrophysics missions and therefore this solution is ruled out.

Regarding the inflatable booms, they have almost the best packaging ratio and a low system complexity. In effect, the boom is deployed by injecting gas in it. Furthermore, the structure is lightweight. However, the rest of the features are not in favour of astrophysics missions. In fact, the latter has a low bending stiffness in spite of the rigidization process. Moreover, it has a low deployment accuracy, post-deployment stability and it cannot deploy heavy structure (only structure below 10 kg) [22]. Accordingly, this solution is not appropriate.

Then, there is the articulated boom, this technology has been used for many space missions and for a variety of applications, for example the Canadarm2. Regarding the astrophysics applications, the latter was studied for two missions, the Far Infra Red Interferometer (FIRI) [29] in which the structure provides a baseline of 30m thanks to two articulated booms of 14m and Advanced Telescope for High Energy Astrophysics (ATHENA) [30] for which the deployable mechanism increases the focal length to 11.5m. Nevertheless, they have never been tested. On one hand, this structure is well suited for astrophysics missions with one of the best deployment accuracy and a very good bending stiffness, nearby 10^7 $N.m^2$ and on the other hand it is one of the heaviest booms with a very bad packaging ratio which is not ideal for our small missions as PROBA-V. Yet, the results shown in these figures are related to much larger booms for our mission. Consequently, the latter is subjected to further analysis.

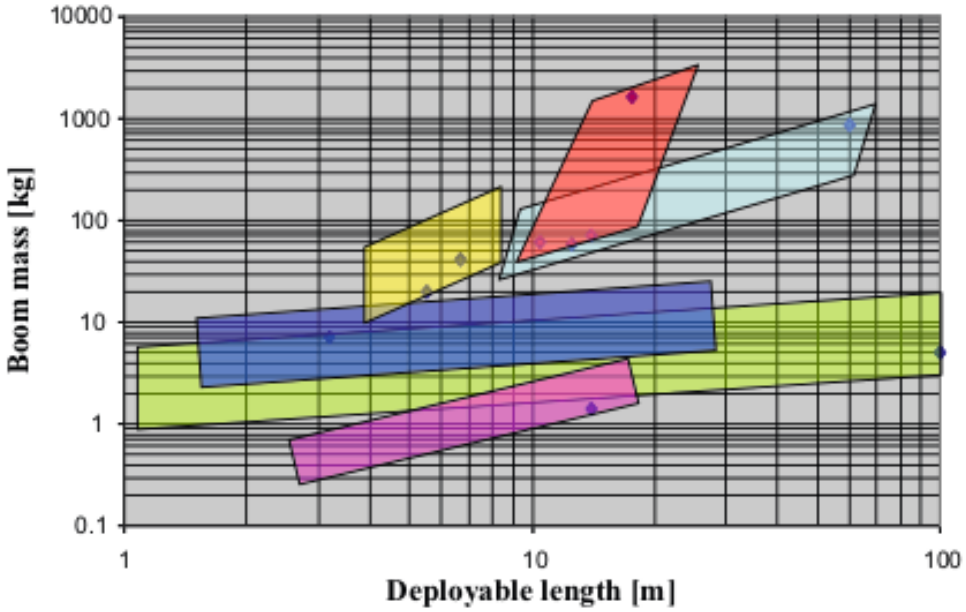

Figure 4.3: Boom mass in function of the deployable length and the type of technology [22].

The telescopic boom has very good qualities for an astrophysics mission. Like the previous boom, this one is not a very lightweight and compact structure. Indeed, with the data available the stowed volume for a 3-meter boom can be estimated to 5.65 $10^{-}3$ m^3 which represents 12% of the total volume. Assuming that the deployment mechanism is composed of at least two booms, 24% of the total volume is used. It is too much considering some other necessary elements for the operation are not include in the estimated volume, such as power systems. Overall, it can be interesting to further study this technology as the data available is extrapolated from one or two designs of larger booms.

Finally, there is the Thin-walled deployable boom. The figures show data for Shape memory composite booms (SMC) and the article includes the Collapsible tube mast in this family of booms. This structure is the lightest structure under 5m length and with a very good packing efficiency. The bending stiffness of this technology is low, which leads to poor precision in the positioning and also a low post-deployment stability. At first sight, this technology does not seems suitable for the small space interferometer, but it allows to modify plenty of parameters in order to adapt the boom for a given application. Moreover, the SMC does not represent only the Thin-walled deployable boom. In conclusion, it is interesting to have a thorough analysis of this technology in order to see if it is adequate for our mission.

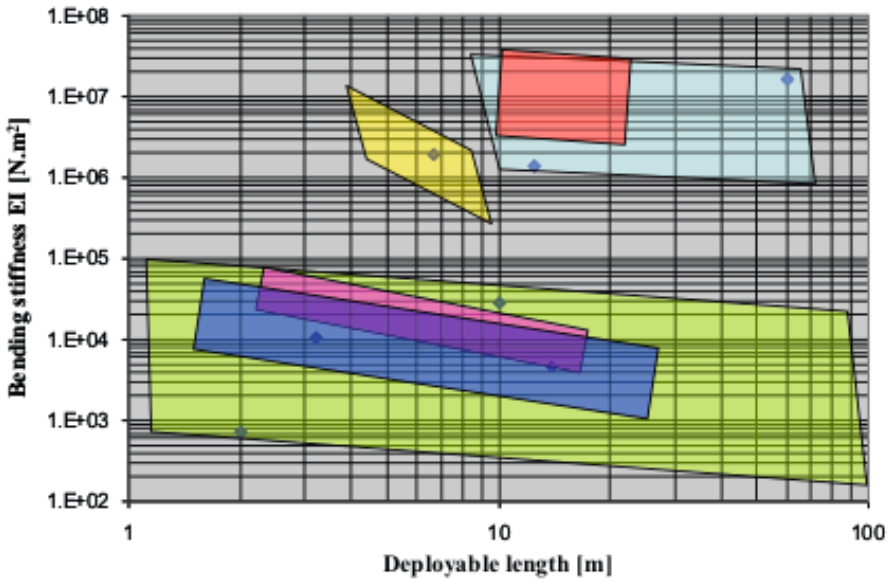

Figure 4.4: Bending stiffness in function of the deployable length and the type of technology [22].

4.2 First pre-design

After the comparison of the technologies with data accessible in the literature, three deployable structures are chosen for a further analysis. Prior to the analysis, a first pre-design of the of the booms is necessary which is presented in this section.

Telescopic boom

The simplified model of the Telescopic boom is represented by the figure 4.5. In the figure 4.5 (a), it can be seen that the structure is composed of 4 hollow tubes , which is an arbitrary choice discussed in the analysis. The diameter at the satellite level is considered to be of 5% of the total length, being 10 cm. Concerning the thickness, each tube has the same thickness and the latter influences directly the radius of the following tubes. A dimensionless number e/r is used to fix it, with e the thickness and r the radius of the first tube. e/r is set to 0.03 which gives a thickness around 1.5 mm. Yet, there is a lower limit of the thickness, indeed the radius of the tube $i+1$ is the radius of the tube i subtracted by the thickness, thus when the thickness enhances, the radius of the following tubes decreases. If the thickness increases to much, the following tubes becomes too small in which case the technology is considered to be not usable. For a

Telescopic boom with 4 segments, the constraint about the thickness can be expressed as

$$e_{max} < \frac{R_{1\_ext} - R_{dep\_syst}}{4} \tag{4.2}$$

where :

- R_{1_ext} is the external radius of the first tube.
- R_{dep_syst} is the minimum radius needed by the deployable mechanism in the last tube.

Regarding the boundary condition, on one side the structure is clamped which represents the satellite side and, on the other side it is free to move, there is also a payload that represents the telescope. Furthermore, each segment has a different diameter and thus, a different linear density. The figure 4.5(b) is a more simplified model used for the analysis. Indeed, the boom is represented by four segments being attached rigidly, without taking into account the effects of the overlap such as the play between adjacent segments. One can also see an applied force F due to the payload, this force is discussed in the next section.

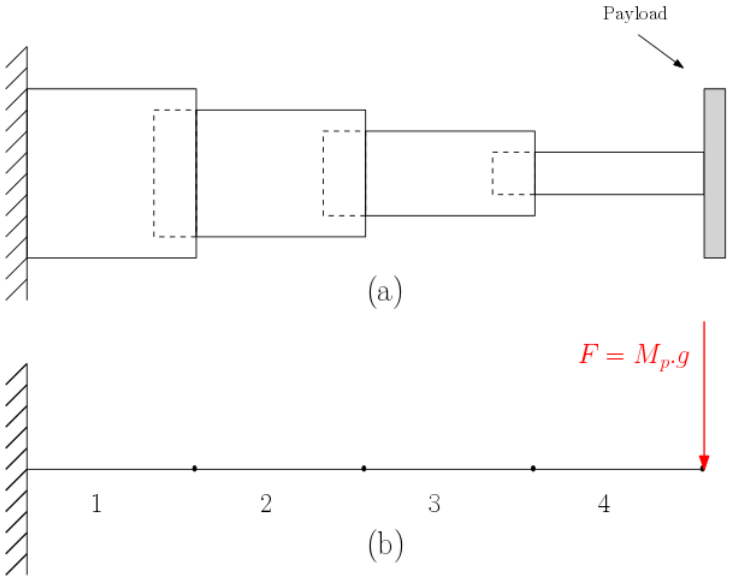

Figure 4.5: Simplified model of the Telescopic boom.

Articulated boom

The simplified model of the articulated boom is illustrated by the figure 4.6 (a). Unlike the Telescopic boom segments, the articulated boom has 3 segments. Indeed the

more segments there are, the more complex the structure is. Therefore, the choice of 3 segments is considered which is discussed in the analysis. Concerning the diameter and the dimensionless number e/r, they are identical to the previous boom. In fact, the aim is to compare the 3 technologies. Contrary to the diameters of the Telescopic boom, the Articulated one have no constraint. Therefore, a constant diameter is taken for the 3 segments. However, this technology is often used with small diameters as a large diameter is not suitable for the folding process of the structure.

The figure 4.6 (b) shows a more simplified model. The assumption of a rigid connection between adjacent boom is made. Respecting the boundary conditions, they are similar to the Telescopic boom. On one side, the boom is clamped to the satellite and, on the other side, it is free to move with the payload.

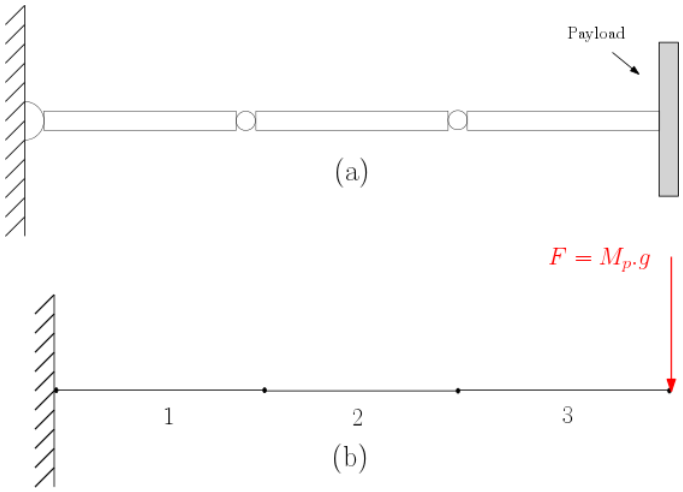

Figure 4.6: Simplify model of the Articulated boom.

Thin-walled deployable boom

This technology is composed of different types of profile discussed in the previous chapter. We are not going to study all of them, the Colapsible Tube Mast seems to be a good choice. Indeed, the latter has closed a cross-section, which gives a good torsional stiffness and the profile will better withstand to buckling under non-axial loading, as mentioned by ZhongYi Chu and YiAn Lei [31]. Before starting the static study of the Collapsible boom, it is necessary to define the profile in order to compute the second moment of area of the cross-section and to determine the maximum stress in the thin strip.

Figure 4.7 illustrates the first quadrant of the Collapsible Tube, as the latter do not have a basic shape, the design of the cross-section is difficult. Therefore, standard design formulae are defined, based on the figure 4.7 which is inspired by F. Hakkak

and S. Khoddam's work [32]. As the structure is symmetrical about its vertical and horizontal axis, only one quadrant is used to define all the cross-section. The red curve is the neutral axis while the green and the blue ones are respectively the inner and outer parts, which defines the thickness of the section. The shape is composed of two circular arcs and one flat edge, the latter is very important as it is used for the manufacturing of the boom. In fact, the boom is made by joining two identical symmetrical lenticular lips as illustrated in Figure 4.8.

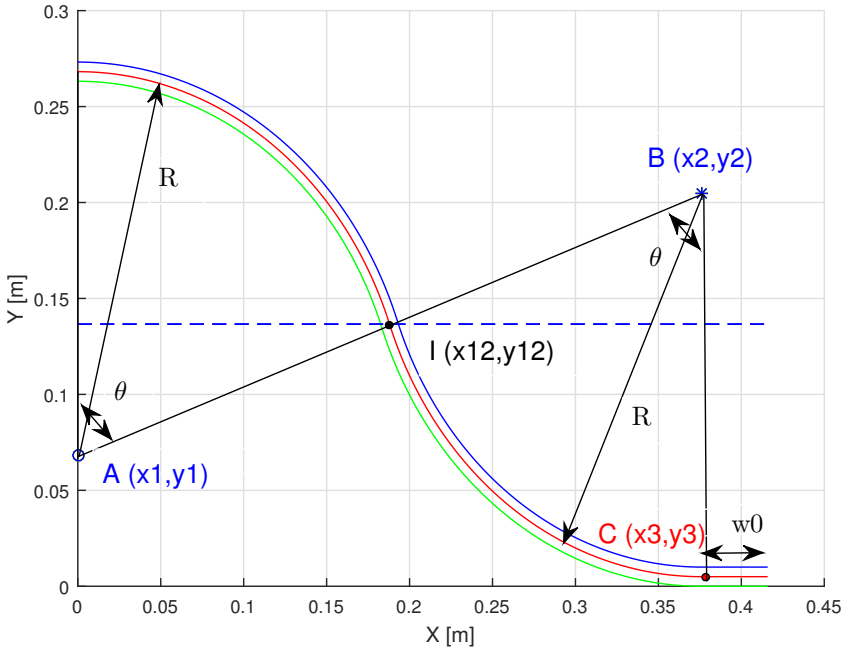

Figure 4.7: First quadrant of the lenticular cross-section of the Collapsible Tube Mast.

Figure 4.8: Lips of Collapsible Tube Mast.

Points A and B are the centre of the first and second circular arc, while point C is the beginning of the flat edge of length w_0. Finally, point I represents the intersection of the two circular arcs. This cross-section is characterised by 3 parameters, the radius, the angle of the circular arcs and the thickness of the curve. In order to use a

simplified model, the angle and the radius of both arcs are similar and the length w_0 is proportional to the radius. By defining these four points, one can be able to design the lenticular curve comfortably, the coordinates of these points can be determined thanks to the following formulae.

$$x_1 = 0 \tag{4.3}$$

$$y_1 = R\left[1 - 2sin\left(\frac{\pi}{2} - \theta\right)\right] + \frac{t}{2} \tag{4.4}$$

$$x_2 = 2\,R\,cos\left(\frac{\pi}{2} - \theta\right) \tag{4.5}$$

$$y_2 = R + \frac{t}{2} \tag{4.6}$$

$$x_{12} = R\,cos\left(\frac{\pi}{2} - \theta\right) \tag{4.7}$$

$$y_{12} = R\left[1 - sin\left(\frac{\pi}{2} - \theta\right)\right] + \frac{t}{2} \tag{4.8}$$

$$x_3 = 2\,R\,cos\left(\frac{\pi}{2} - \theta\right) + w_0 \tag{4.9}$$

$$y_3 = \frac{t}{2} \tag{4.10}$$

Now the profile is defined, the moment of area can be computed by using a quarter of the section and multiplying the results by a factor 4, for the same reason. The moment of area along x-axis can be computed as [32]

$$I_{xx} = 4\int_0^{x_1} t\,r_1\,\frac{\left(\sqrt{r^2 - x^2} + y_1\right)}{\sqrt{r^2 - x^2}}dx + 4\int_{x_1}^{x_2} t\,r\frac{\left(-\sqrt{r^2 - (x - x_2)^2} + y_2\right)^2}{\sqrt{r^2 - (x - x_2)^2}}\,dx \tag{4.11}$$

When the integrals are computed, the equation becomes

$$I_{xx} = 2\,t\,r\left[x_1\sqrt{r^2-x_1^2} + (r^2+2\,y_1^2)sin\left(\frac{x_1}{r}\right)^{-1}\right] + 2\,t\,r\,(x_2-x_1)\left[\sqrt{r^2-(x_2-x_1)^2}\right.$$
$$\left. - 4\,r + 6\,t\,r^3\,sin\left(\frac{x_2-x_1}{r}\right)^{-1} + 8\,t\,r\,x_1\,y_1\right.$$

A similar method gives the moment of area about y-axis

$$I_{yy} = 4\int_0^{x_1} t\,r\,\frac{x^2}{\sqrt{r^2-x^2}}\,dx + 4\int_{x_1}^{x_2} t\,r\,\frac{x^2}{\sqrt{r^2-(x-x_2)^2}}\,dx + 4\int_{x_2}^{x_3} t\,x^2\,dx \quad (4.12)$$

By computing the integrals, the equation becomes

$$I_{yy} = 2tr\left[r^2\,sin\left(\frac{x_1}{r}\right) - x_1\sqrt{r^2-x_1^2}\right] + \frac{4t}{3}(x_3^3-x_2^3) + 2tr\left[(3x_2+x_1)\sqrt{r^2-(x_2-x_1)^2}\right.$$
$$\left. - 4x_2r + 2tr(2x_2^2+r^2)sin\left(\frac{x_2-x_1}{r}\right)^{-1}\right.$$

The method of storage of this technology is very specific, the thin strip is first flattened and then it is wrapped around a storage reel of radius R_s. The strip has to be deformed elastically in order to recover its shape once deployed. Therefore, it is important to check the maximum stress in the Thin-walled boom.

The first stress occurs during the flattening, Figure 4.9 illustrates the cross section of the strip with an angle α, which is equal to 2θ, a thickness e and a radius R which is assumed to be much larger than the thickness of the boom. During the flattening, the neutral fibre stays unstrained unlike the upper and inner fibre. The new lengths of the different fibres are the following

$$\begin{aligned} Neutral\ fibre : l &= \alpha R \\ Upper fiber\ : l^u &= \alpha\left(R+\frac{e}{2}\right) \\ Inner fiber\ : l^i &= \alpha\left(R-\frac{e}{2}\right) \end{aligned}$$

The strain in the upper fibre is

$$\epsilon = \frac{l^u - l}{l} = \frac{\left(R+\frac{e}{2}\right)-R}{R} = \frac{e}{2R}$$

The maximum stress after flattening is the following, where E is the Young's Modulus and the latter must be lower then the yield strength R_e.

$$\begin{aligned} \sigma_{max} = E\epsilon_{max1} &= \frac{Ee}{2R} < R_e \\ \iff \frac{e}{r} &< \frac{2R_e}{E} \end{aligned} \tag{4.13}$$

Then, the second stress arises when the thin strip is wrapped around the storage reel of radius R_s, the stress is along the axial axis. The maximum stress after coiling will be

$$\begin{aligned} \sigma_{max} &= \frac{Ee}{R_s} < R_e \\ \iff \frac{R_s}{e} &> \frac{E}{R_e} \end{aligned} \tag{4.14}$$

The relation 4.13 and 4.14 are dimensionless indicators that give two geometric constraints. Indeed, the first one can be seen that for a given radius, the Collapsible Tube Mast has a maximum thickness. While, the second one is for a given thickness, there is a minimum radius of storage reel.

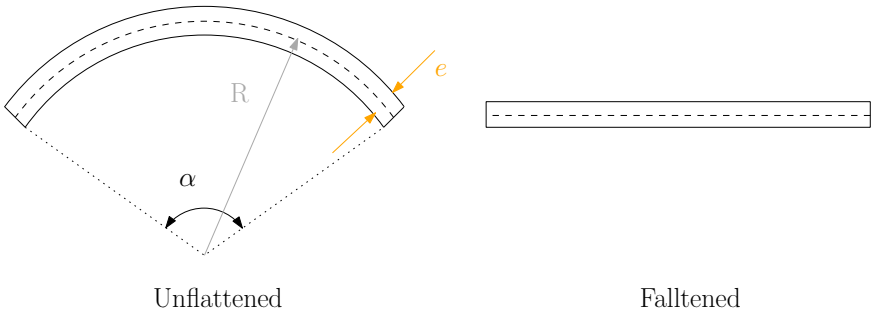

Figure 4.9: Cross-section of radius R and angle α.

Finally, Figure 4.10 (a) illustrates the simplified model of the Thin-walled deployable boom. This is a configuration similar to a cantilever beam. Regarding the

diameter, it is the same as the two other booms, while the thickness is different. In fact, for a good comparison it is preferable to have the same geometric dimensions but, in the case of Collapsible Tube Mast, there is a constraint limiting the thickness, given by equation 4.13. With the material properties of Aluminum 7050 and by taking a safety factor of 0.95, the maximum thickness is limited by

$$e_{max} = r\frac{2R_e}{E}0.9 = r\ 0.0106 \tag{4.15}$$

With a radius of 5 cm, thickness is of approximately 0.53 mm, at the most. The figure 4.10 (b) shows a more simplified model containing the same boundary conditions as for the Telescopic and Articulated booms.

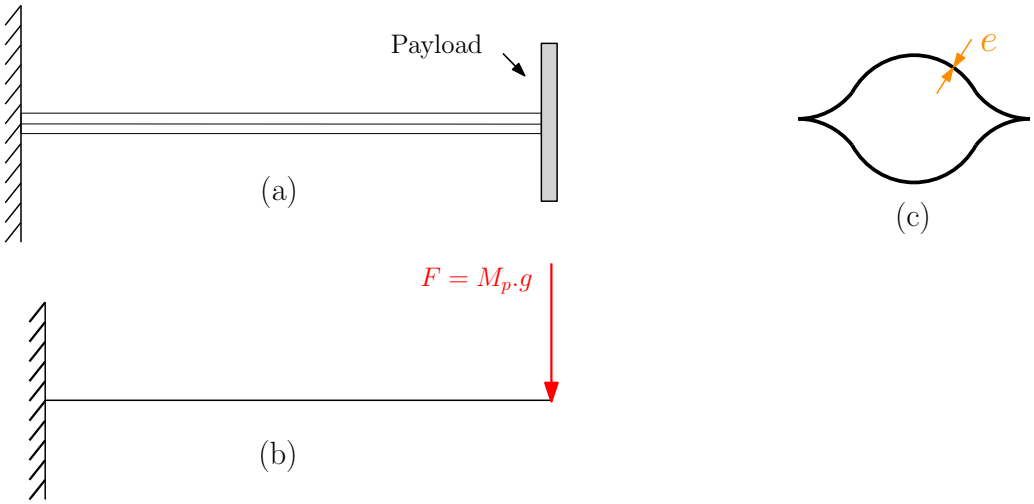

Figure 4.10: Simplified model of the Thin-walled deployable boom.

4.3 Static analysis of the selected technology

In this section, the static analysis of these three technologies is done, the Telescopic boom, the Articulated boom and the Collapsible Tube Mast. Prior to the analyses, the static load case is defined. The aim is to compare the stiffness of the different technologies in order to find which technology maximises the stiffness while minimizing the bulk and the weight.

4.3.1 Load case

In space, the structures are not subjected to gravity, that is why some systems such as the Canadarm2 fulfills their tasks in space very well but they can even not carry their own weight on Earth. However, the satellite can be subjected to some perturbations which leads to a deviation of the satellite from the set trajectory or the target can be deviated from the viewfinder. Thus, a readjustment manoeuvre is needed. Therefore, the representative case of an angular motion manoeuvre from the attitude control system is taken, this motion is provided with flying wheels that give an angular acceleration and that induces a load, which is used for this static analysis.

In order to determine the load applied on the structures, the angular acceleration has to be defined. It is assumed that the satellite can be adjusted by 1 degree per second. Figure 4.11 shows a smooth trajectory of the angle changing by 10 degree in 10 seconds, while the figure 4.12 and 4.13 respectively illustrates the evolution of the angular speed and the angular acceleration needed. It can be seen that the satellite is subjected to a maximum acceleration of 0.01 rad/s. The response of this acceleration on the structures are now studied.

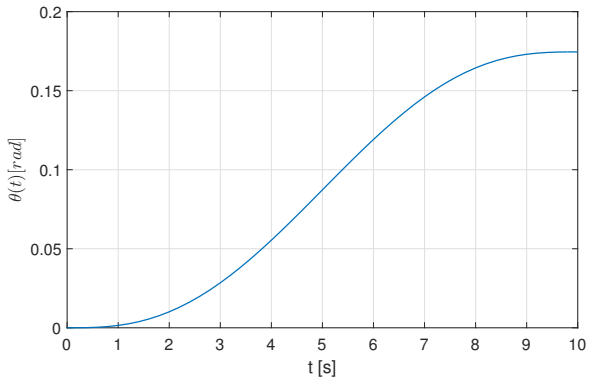

Figure 4.11: Smooth evolution of angle in function of the time.

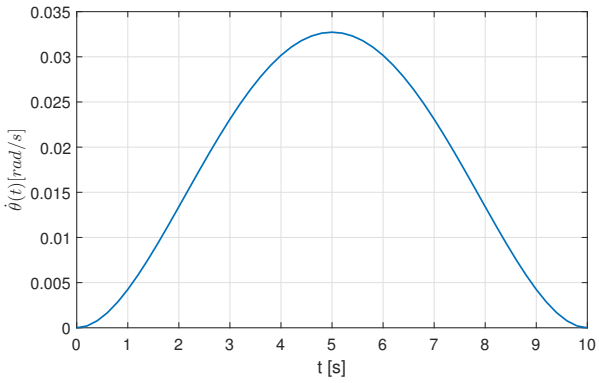

Figure 4.12: Evolution of angular speed in function of the time.

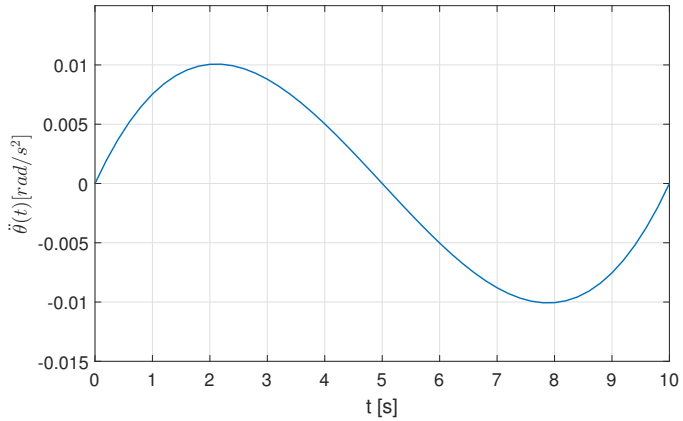

Figure 4.13: Evolution of the angular acceleration in function of the time.

4.3.2 Telescopic boom

The deflection of the Telescopic boom is computed thanks to the Euler-Bernoulli Beam theory. Indeed, the deflection of the boom is considered to be small and the boom is only subjected to transverse loads. The Euler-Bernoulli equation allows to determine the deflection

$$\frac{d^2}{dx^2}\left(EI\frac{d^2v}{dx^2}\right) = p \tag{4.16}$$

Where :
- $v(x)$ is the boom deflection
- $p(x)$ is the distributed load
- E is the Young's Modulus
- I is the second area of moment

After the integration of the equation 4.16 twice and with the assumption of linear elastic material, it gives the following non linear, second order, ordinary differential equation

$$\frac{d^2v}{dx^2} = -\chi = \frac{M}{EI} \tag{4.17}$$

where χ is the curvature of the boom.

The equation 4.17 is resolved four times, for each segment, to obtain the overall transverse displacement. However, it gives 8 expressions with 8 unknowns and the latter

are determined by means of the following boundary conditions, which represent angles and displacements continuity between adjacent segments.

$$v_1(0) = 0 \tag{4.18}$$

$$\frac{dv_1(0)}{dx} = 0 \tag{4.19}$$

$$\frac{dv_1(l/4)}{dx} = \frac{dv_2(0)}{dx} \tag{4.20}$$

$$v_1(l/4) = v_2(0) \tag{4.21}$$

$$v_2(l/4) = v_3(0) \tag{4.22}$$

$$\frac{dv_2(l/4)}{dx} = \frac{dv_3(0)}{dx} \tag{4.23}$$

$$v_3(l/4) = v_4(0) \tag{4.24}$$

$$\frac{dv_3(l/4)}{dx} = \frac{dv_4(0)}{dx} \tag{4.25}$$

First, the curvature has to be determined, in other words the moments and forces acting within the beam. The latter are evaluated by using free-body diagrams of each section, the computation of the fourth segment is illustrated below and the details for the other segments can be found in Appendix A.

The fourth segment

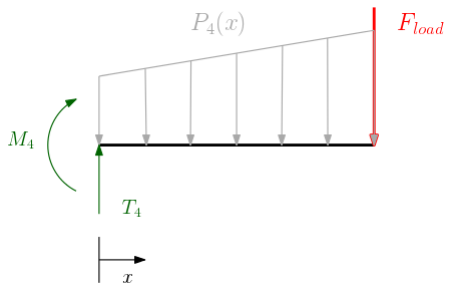

with :

-$F = M_{load}.l.\ddot{\alpha}$
-$P_4(x) = S_4.\rho.\ddot{\alpha}.\left(x + \frac{3l}{4}\right)$

Figure 4.14: Free body diagrams of the fourth section of the boom.

where :
- M_load is the mass of the payload.
- $\ddot{\alpha}$ is the angular acceleration.
- S_4 is the cross-section area of the fourth segment.
- ρ is the density of the material.
- l is the total length of the boom, 2 meters.

$$T_4 = F + \int_0^{l/4} P_4(x)dx = M_{load}l\ddot{\alpha} + S_4\rho\ddot{\alpha}\frac{7l^2}{32}$$
$$M_4 = -F\frac{l}{4} - \int_0^{l/4} P_4(x)xdx = -\frac{m_{load}\rho.\ddot{\alpha}l^2}{4} - S_4\rho.\ddot{\alpha}\frac{11l^3}{384}$$

Therefore, moments and forces acting within the fourth boom segment are given by

$$T_4(x) = T_4 - S_4\rho\ddot{\alpha}\left(\frac{x^2}{2} + \frac{3lx}{4}\right) = M_{load}\rho\ddot{\alpha} + S_4\rho\ddot{\alpha}\left(\frac{7l^2}{32} - \frac{x^2}{2} - \frac{-3lx}{4}\right)$$
$$M_4(x) = M_4 - \int_0^x P_4(x)xdx + T_4x = M_{load}\ddot{\alpha}\left(lx - \frac{l^2}{4}\right) + S_4\rho\ddot{\alpha}\left(-\frac{x^3}{3} - \frac{-3lx^2}{8}\right)$$
$$+ S_4\rho\ddot{\alpha}\left(\frac{7l^2x}{32} - \frac{11l^3}{284}\right)$$

Now that the internal moment and forces for the entire boom is known, the angle of deflection θ and the transverse displacement v can be computed thanks to equation

4.17 (solution is presented in Appendix A) and the 8 boundary conditions. The resolution is done via *MATLAB* with the function **Telescopic_static_analysis.m** .

The deflection of the Telescopic boom is illustrated in Figure 4.15 with the values of parametric variables fixed in the previous section. The final deflection is about -7.61 $10^{-6}m$, which is small. The latter will be compared to other boom deflections. It can be interesting to compare the bending stiffness, boom mass and the packaging ratio with the one discussed in the review on large deployable structure [22].

At first, the bending stiffness of the boom is about 1.27 10^4 N/m^2 which is much lower than the values present in Figure 4.4. However, the boom diameter uses is also smaller than the article. Indeed, the bending stiffness shown in the figure is the one of the ISIS Telescopic boom designed by Northrop Grumman with an average diameter larger than half a meter. Nevertheless, the bending stiffness of our boom is overestimated. In order to simplify the study, the assumption of rigid connection between adjacent segments is taken. In reality the connections of the adjacent tubes are made by an overlapping of the first tube on the second one, which gives a lower stiffness than a rigid connection.

Then, the boom mass is approximately 2.5 kg, which is also lower than expected. This weight represents approximately 2% of the reference weight of the PROBA-V mission. Nonetheless, it should be noted that there are other elements, such as actuators, control mechanisms that are not included in this weight, so it is underestimate.

Finally, the packaging ratio is about 0.3 which is a bit above the result of Figure 4.2. Nevertheless, the packaging ratio depends on the number of segments, a better packaging ratio can be obtained by increasing the number of tube segment for a given boom length. On one hand, it is necessary to increase the boom radius to maintain the same bending stiffness, which makes the structure heavier and on the other hand, tube thickness can be decreased, which reduces the weight but makes the structure less stiff.

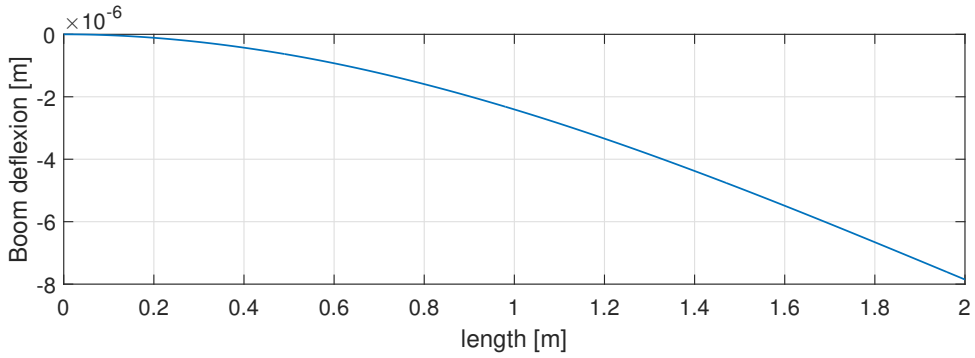

Figure 4.15: Deflection of the Telescopic boom under an angular acceleration of 0.01 rad/s^2.

4.3.3 Articulated boom

The study of the Articulated boom is nearly similar to the previous case. That is why, the development is not described. The resolution is done via *MATLAB* with the function **Articulated_static_analysis.m**

The deflection of the Articulated boom is illustrated in Figure 4.16. It can be seen that the final deflection is about $-7.54\ 10^{-6}\ m$ that is of the same order of magnitude as the Telescopic boom. Concerning the bending stiffness, the latter is about $1.33\ 10^4\ N/m^2$ which is much lower than the extrapolated results of Figure 4.4 and the explanation is the same as for the bending stiffness of the Telescopic boom. Once again, the assumption of rigid connection does not reflect the reality. Usually, the arm is put in motion by actuators, such as motors located between two adjacent rigid parts. The latter define the stiffness of the connections and also the maximum load the arm can carry. These actuators have a significant weight, which is not considered in the static study. Therefore, the bending stiffness is overrated.

Next, the boom weight is 2.64 kg which is a little bit heavier than the Telescopic boom. Moreover, it is even more underestimated as actuators for this technology outweighs the previous one.

In the end, the packaging ratio is 0.33, which is under the extrapolated results. It represents the ratio between the deployable length and the stowed length and is influenced by the number of segments. More segments means a more complex system, and consequently a less reliable deployment. However, the storage volume is a very important factor as for this technology, it does not depend on the number of segments. This volume is about 0.0157 m^3 for one arm which is three times bigger than the Telescopic boom and it represents 3% of the reference volume, PROBA-V platform.

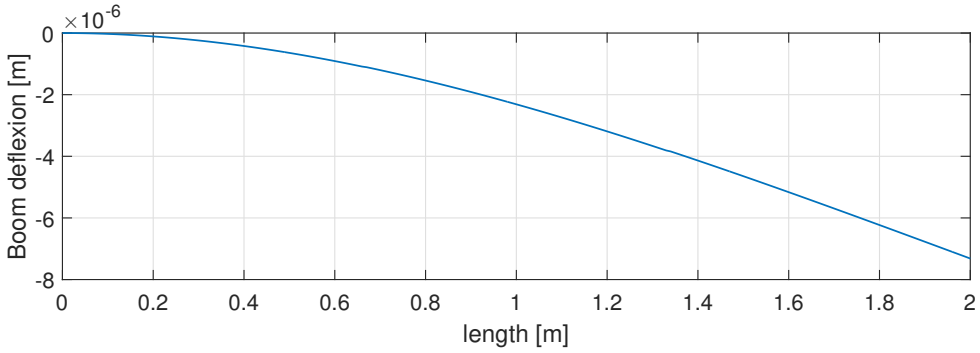

Figure 4.16: Deflection of the Articulated boom under an angular acceleration of 0.01 rad/s^2.

4.3.4 Collapsible Tube Mast

The study of the Collapsible Tube Mast is simple once the section properties are determined. The development of the solution is not described as it is similar to the Telescopic boom. Unlike other booms, the collapsible Tube Mast has a constraint regarding the thickness. Indeed, as the latter is flattening during the storage process, it is essential to avoid yielding. Thus, for a radius of 5 cm, the thickness is fixed to 0.4 mm, which is lower than the limiting value of 0.53 mm given by the relation 4.15. The resolution is done via *MATLAB* with the function **CTM_static_analysis.m** .

Unlike the Telescopic and Articulated boom stiffness, this boom has different bending stiffness depending on the axes, the stiffness along the y axis is about 1.3607 10^4 N/m^2, which is of the same order of magnitude as the other two booms, while, along the x axis it is 4.0573 10^3 N/m^2, which is one order of magnitude lower. Compared to the results of Figure 4.4, the bending stiffness along y axis is in accordance. The deflection of the Collapsible Tube Mast is displayed in Figure 4.17. The maximum deflection along the x axis is about -7.34 10^{-6} m, whereas along the y axis, it is -2.46 10^{-5} m. However, the boom is not totally clamped at one side, after the retractable/deployable mechanism there is a support collar which blocks the boom and depending on the design of the latter, the boom can have some play. Consequently, the deflection is overvalued.

The Collapsible Tube Mast is an extremely lightweight structure. Indeed, the latter only weighs 1 kg for a 2-metre length, which is twice less than the other boom weight. Nonetheless, the deployment mechanisms weight is not taken into account.

Concerning the packaging ratio, the latter is about 0.156, which is also almost

half the previous deployable boom ratios. This value is bigger than the results of Figure 4.2. In fact, the packaging of this structure depends mainly on the storage reel diameter, this diameter should be big enough to avoid yielding in the strip during the wrapping. The relation 4.17 gives the minimum storage reel radius R_s needed to wrap the strip elastically. With Aluminum 7050 and a thickness of 0.4 mm the radius should be larger than $7,1$ cm. However, by using materials with a higher yield strength, it is possible to have a more compact system. Indeed, Carbon Fibre Reinforced Plastic composites (CFRP) allows to build a stiffer, more lightweight and more compact boom with a yield strength twice as the Aluminum 7050 one, approximately about 985 N/mm^2.

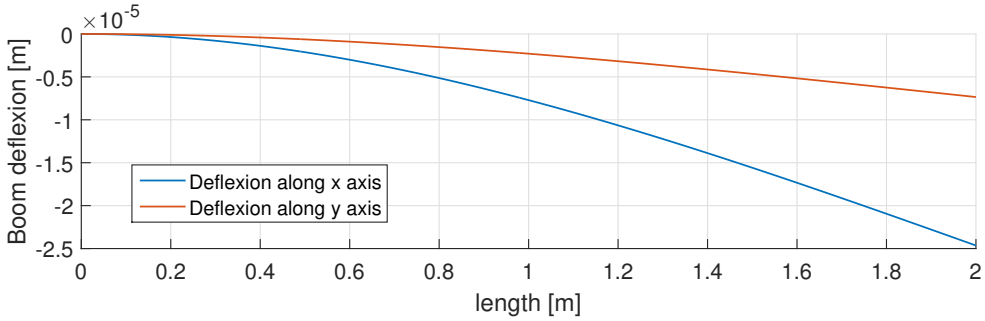

Figure 4.17: Deflection of the Collapsible boom under an angular acceleration of 0.01 rad/s^2.

4.4 Modal analysis

In this section, the modal analysis is done in order to compute the eigen frequencies of the three technologies. The aim is to find which technology has the highest first eigen frequency for a minimum bulk and weight. This computation is done in 3 steps. First, it is necessary to model the structure, unlike the static analysis that is done analytically, the model analysis is done by finite elements in *MATLAB* by using "*3D beam finite elements*". After the modelling, the structural stiffness and mass matrices are built. Finally, the eigen frequencies and their relative mode shape are determined. Only the development for the Telescopic boom is described, as the other booms have a similar resolution. This method is inspired from Mechanical Vibration [33].

4.4.1 Modelling

The discretization is based on the model of Figure 4.5. The structure is divided in 4 segments representing the elementary beams, the latter are re-divided in Ndiv elements, which gives Ndiv-1 new nodes. This operation is done in **elements.m**.

Since the structure is in 3D, each node has six degrees of freedom (DoFs), in fact three degrees of freedom for translation and three for the rotation. As each element is composed of 2 nodes, which gives 12 DoFs per element and the vector is represented by q_{el}^T. The line represents the element and the columns its DoFs. This step is carried out in **list_dof.m**.

$$\mathbf{q}_{el}^T = [u_1 \;\; v_1 \;\; w_1 \;\; \gamma_{x1} \;\; \gamma_{y1} \;\; \gamma_{z1} \;\; u_2 \;\; v_2 \;\; w_2 \;\; \gamma_{x2} \;\; \gamma_{y2} \;\; \gamma_{z2} \;]$$

Each element has a local axes system, the **x** axis is the main axis of an element and the two other axes depend on the orientation of the structural axes.

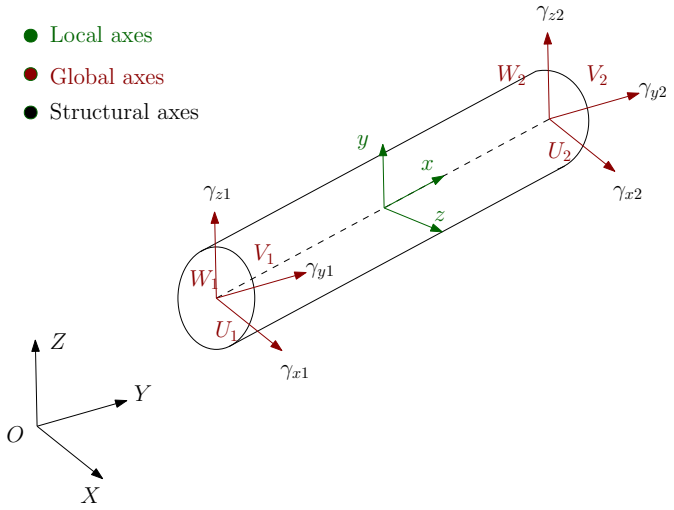

Figure 4.18: The local axes of an element.

4.4.2 Determination of $\mathbf{K_s}$ and $\mathbf{M_s}$

In order to determine the structural stiffness and mass matrices, the elementary stiffness $\mathbf{K_{el}}$ and mass $\mathbf{K_{el}}$ matrices are constructed, these matrices are presented in Appendix B. They are calculated by the function **matrix_KM_el.m** .

Then, these matrices are expressed in structural axes thanks to the transformation matrix $\mathbf{T_el}$, the latter makes it possible to pass from local axes to global axes. Indeed, adding matrices that have frame of reference oriented in a different direction would not be meaningful. The DoFs, the stiffness and the mass matrices of each element can be expressed in the structural axes as following

$$\mathbf{q_{el}} = \mathbf{T_{el}}.\mathbf{q_{eS}} \qquad \mathbf{K_{eS}} = \mathbf{T_{el}^T}.\mathbf{K_{el}}.\mathbf{T_{el}} \qquad \mathbf{M_{eS}} = \mathbf{T_{el}^T}.\mathbf{M_{el}}.\mathbf{T_{el}}$$

with $\mathbf{T_e}$ defined as

$$\mathbf{T_e} = \begin{pmatrix} \mathbf{R_e} & 0 & 0 & 0 \\ 0 & \mathbf{R_e} & 0 & 0 \\ 0 & 0 & \mathbf{R_e} & 0 \\ 0 & 0 & 0 & \mathbf{R_e} \end{pmatrix}$$

The transformation matrix is composed of rotation matrices $\mathbf{R_{el}}$, the latter is expressed as following, where x,y and z are the local axes and X, Y and Z are the structural axes. This operation is done by the function **matrix_TT.m** .

$$\begin{pmatrix} x_i \\ y_i \\ z_i \end{pmatrix} = \mathbf{R_e} \begin{pmatrix} X_i \\ Y_i \\ Z_i \end{pmatrix} (\mathbf{i = 1, 2})$$

Lastly, the structural stiffness and mass matrices are built by assembling all the stiffness and mass matrices (in the structural axes). The assembly is carried out thanks to the localisation matrix $\mathbf{L_k}$. This matrix has a size of [number of elements $\times$ DoFs of an element], it contains only Boolean values and it enables to put each element matrix in a global set allowing the continuity of the overall structure. In other words, it allows to know which DoF, in the nodal displacement, corresponds to the DoF of the element. This process is performed by the function **matrix_KM_s.m** .

$$\mathbf{K_S} = \sum_{\mathbf{k=0}}^{\mathbf{Nelem}} \mathbf{L_k^T}.\mathbf{K_k}.\mathbf{L_k} \qquad \mathbf{M_S} = \sum_{\mathbf{k=0}}^{\mathbf{Nelem}} \mathbf{L_k^T}.\mathbf{M_k}.\mathbf{L_k}$$

$$\mathbf{q_{eS}} = \mathbf{L_k}.\mathbf{q_S}$$

4.4.3 Eigen frequencies

The eigen frequencies are determined with the Lagrange equation and we obtain

$$\begin{aligned} & \mathbf{M_S}.\ddot{\mathbf{q}} + \mathbf{K_s}.\mathbf{q} = \mathbf{0} \\ \Leftrightarrow\ & \mathbf{K_S}.\mathbf{x} = \boldsymbol{\omega}^{\mathbf{2}}.\mathbf{M_S}.\mathbf{x} \end{aligned}$$

This equation allows to determine the pulsation ω [rad/s] of the structure and the corresponding eigenvectors $\mathbf{x}$. The eigen frequencies are obtained by dividing ω by 2π, while the eigenmodes are normalized in order to distinguish the shape correctly. This operation is carried out in **frequencies.m** .

It can be seen by some verifications if the structural stiffness and the structural mass matrices are correctly implemented.

- First, one can verify if the elementary stiffness and mass matrices are well assembled by checking the symmetry of the structural matrices. $\|\mathbf{K_S^T} - \mathbf{K_S}\|$ must give a matrix fulfilled with zeros and the same operation can be repated for structural mass matrix. However, the result is not exactly a zero matrix, which is due to the fact that there are some numerical inaccuracies. Thus, the symmetry can be verified by checking that the maximum of $\|\mathbf{K_S^T} - \mathbf{K_S}\|$ does not exceed, for example, 10^{-8}.

- Then, in order to check if $\mathbf{K_S}$ and $\mathbf{M_S}$ are well computed, one can verify the orthogonality of the eigenmodes:

$$\mathbf{q_k}.\mathbf{K_s}.\mathbf{q_l} = \gamma_\mathbf{j}.\delta_\mathbf{kj}$$
$$\mathbf{q_k}.\mathbf{M_s}.\mathbf{q_l} = \mu_\mathbf{j}.\delta_\mathbf{kj}$$

  where
  - γ_j is the generalized stiffness.
  - μ_i is the generalised mass.
  - δ_{kj} is the Kronecker symbol.

  One can verify that γ_j/μ_j is equal to ω_j^2, which is the case.

- Finally, the boundary conditions have to be applied after the computation of matrices $\mathbf{K_S}$ and $\mathbf{M_S}$. The rank of those matrices is checked to make sure that rigid body modes are deleted. To check these conditions, rank of matrices is computed with the MATLAB function *sprank* and it is subtracted to the size of the matrices. The result is of course zero. All those tests are performed in ***verif.m***.

4.4.4 Results

The eigen frequencies are computed for the three technologies, the geometric and material properties are identical to the static analysis. The Table 4.1 illustrates the first five eigen frequencies for the technologies. One can notice that the Telescopic and the articulated boom have identical eigen frequencies for the first and second mode. In fact, this is due to the fact that the second moment of area in the two main directions are identical, unlike the second moment of area of the collapsible Tube Mast.

Moreover, the Collapsible Tube Mast has the lowest first eigen frequency, while the Articulated has the highest one. This is consistent with the bending stiffness of the booms. In effect, the Collapsible Tube Mast has the lowest bending stiffness along x and the first frequency corresponds to the bending along this axis. Whereas, the stiffness in

the y direction is in the same range as the stiffness of other booms which gives a second eigen frequency close to the other boom ones.

Eigen frequencies [Hz]	Telescopic boom	Articulated boom	Collapsble Tube Mast
f_1	9.3207	8.378	4.593
f_2	9.3207	8.378	8.412
f_3	118.688	112.206	80.088
f_4	118.688	112.206	146.669
f_5	277.211	271.035	207.776

Table 4.1: Eigen frequencies of the Telescopic boom, Articulated boom and Collapsible Tube Mast.

4.5 Comparison

In the previous sections, the static analysis and the modal analysis are carried out and the results are discussed. However, the geometric parameters are taken arbitrarily and depending on these values, one technology can seem better than another one. However, this is not a good way to compare the different mechanisms and to find out which one fulfills the requirements the best. In this section, the values of the geometric parameters are varied. On one hand the relation between stiffness, compactness and the weight of the system is studied and, on the other hand, the first eigen frequency is analysed to find out the best technology.

4.5.1 Static analysis results

The aim is to figure out which technology gives a good stiffness with a minimum weight and bulk. For a given stiffness, the weight is compared to the occupied surface by the boom at the satellite side. In fact, since the cross-section of the Collapsible Tube Mast does not only depend on the radius, the latter is not suitable to describe the bulk.

The Figure 4.19 illustrates the occupied surface by the boom in function of the weight for a fixed bending stiffness of the two booms and of the Collapsible mast in the y-axis. The stiffness is set to 2 10^4 N/m^2. It can be seen that the mass rises when the occupied surface decreases and, conversely, when the weight reduces, the occupied surface enhances. Indeed, the parameter which is manipulated to adjust this bending stiffness for a given radius is the thickness of the boom. When the radius increases, a lower thickness is necessary to obtain the fixed bending stiffness, consequently the cross section area also reduces, which leads to a decrease of the total weight.

The Telescopic and the Articulated booms have similar surface area and weight values. The Articulated boom is often used with a low radius, as explained in the first pre-design of the boom. Thus, it is better to choose this technology if occupied area by the boom on the satellite needs to be minimised. Unlike the Articulated boom, the Telescopic one can be used with a larger diameter and the latter does not interfere with the deployment and retractable mechanism. This technology is used when the weight minimisation is more important than the reduction of the bulk. Thus, these structures are complementary.

One can see that the Collapsible Tube Mast (CTM) is the lightest for a given occupied surface and bending stiffness in the y-axis. However, as mentioned in the previous chapter, the CTM has a constraint on the thickness. In effect, this constraint can be visualised by the dashed olive-green line in the figure. Below this line, the value of the radius and the thickness do not allow the strip to flatten without yielding. Therefore, it is better to consider values under this dashed line as not reachable. As mentioned in the pre-design, the CTM does not have the same bending stiffness in its two main directions. The stiffness in the x-axis is lower than the other one, this is illustrated in Figure 4.20. Even in this situation, the Collapsible mast is a little bit lighter than the other technologies. In consequence, the CTM is the best choice if we want to have a lightweight system whatever the boom radius.

The figures 4.21 shows the impact of increasing the bending stiffness. In fact, it illustrates the occupied area in relation to the weight for a fixed bending stiffness of 10^5 N/m^2 . When the bending stiffness increases, on one hand, the dashed olive-green line goes up which reduces the possibility to use Collapsible Tube Mast with lower surface area and, on the other hand, the curves of the three technologies draw away, which gives heavier and more cumbersome structures.

One can observe that the gap between the Collapsible technology and the two other technologies increases for a higher values of bending stiffness. However, the deployment and retractable mechanism increases with the occupied area of the Collapsible mast, this mechanism has a significant weight for a large diameter, which is not taken into account in this study.

An important remark has to be made, when the thickness declines too much, there is a risk of local deformation of the cross section that leads to the collapsing of the structure. The latter is not studied in this thesis.

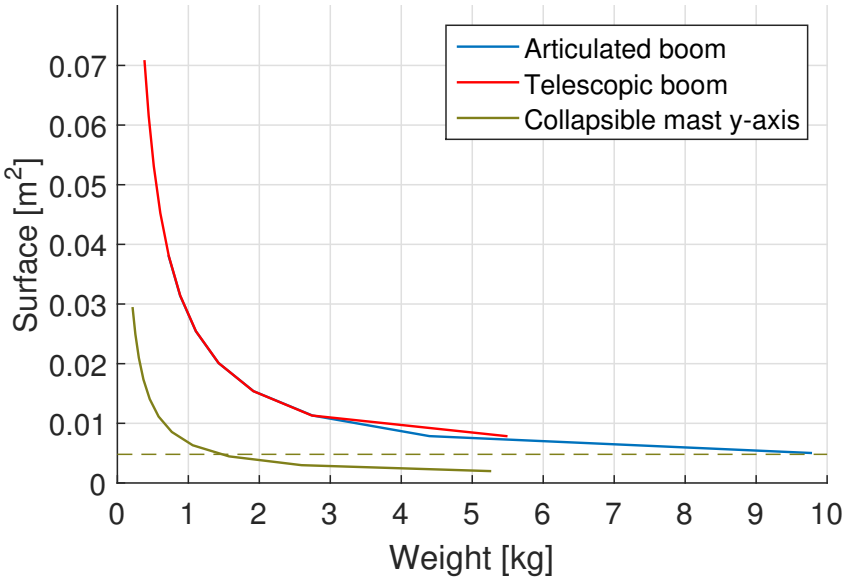

Figure 4.19: Occupied area in function of weight for the bending stiffness 2 10^4 N/m^2 of the y-axis of the Collapsible Tube Mast, the bending stiffness of the Articulated and the Telescopic boom.

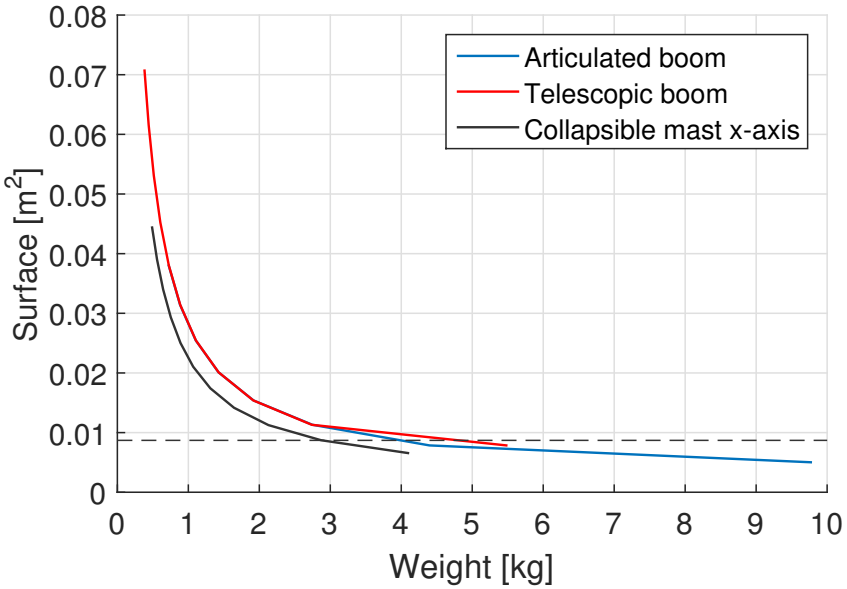

Figure 4.20: Occupied area in function of weight for the bending stiffness 2 10^4 N/m^2 of the x-axis of the Collapsible Tube Mast, the bending stiffness of the Articulated and the Telescopic boom.

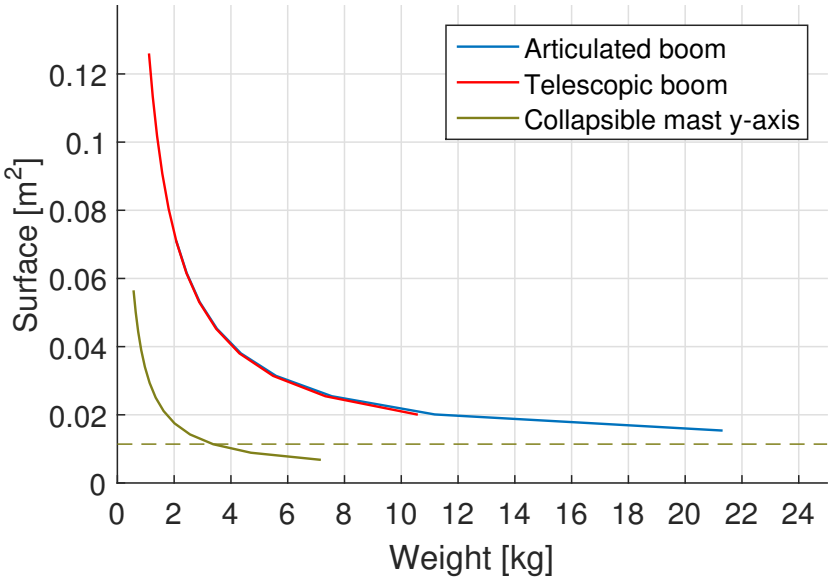

Figure 4.21: Occupied area in function of weight for the bending stiffness 10^5 N/m^2 of the y-axis of the Collapsible Tube Mast, the bending stiffness of the Articulated and the Telescopic boom.

4.5.2 Modal analysis results

In this subsection, a similar comparison is made in order to find the technology that has the minimum cumbersome and weight for a given first eigen frequency.

It can be seen in Figure 4.22 that the results of the three booms are very close, with a Collapsible Tube Mast that is slightly more lightweight than the other, for a given occupied area. In fact, as explained in the Modal analysis section, the first frequency is related to the bending mode along x-axis. This is in accordance with the result of bending stiffness in the x-axis, which gives almost similar weight and cumbersome for a given stiffness. However, at a resonance frequency of 10Hz, it is not possible to use this technology with an occupied surface under 8.7 10^{-3} m^3, which corresponds to a radius of 7 cm. Even though the weight is low, a diameter of 14 cm is too large for a 2-meter length boom.

The three technologies are on the same level concerning the weight and the occupied surface for a given frequency. However, the constraint about the thickness on the Telescopic and the Collapsible Tube Mast does not allow to use a radius as small as the articulated boom one. The conclusion is almost similar to the bending stiffness case. The Articulated boom is well suited if small boom diameter is needed, while the

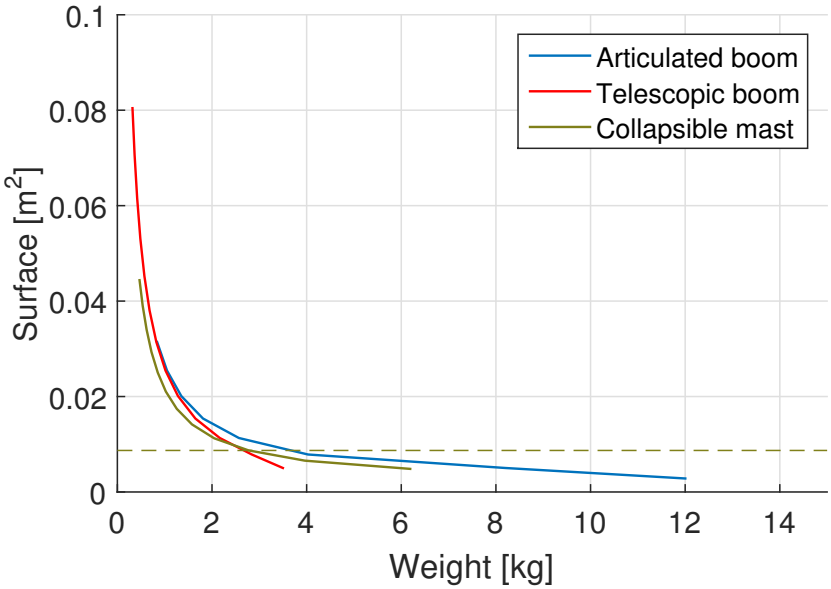

Figure 4.22: Occupied area in function of stowed volume for a first resonance frequency of 10 Hz.

Collapsible is appropriate if low weight is requested.

However, the Telescopic boom seems to be the most compact solution in this case, with a weight of 3.5 kg and a boom diameter of 6 cm. Finally, as for the bending stiffness, if a better desired resonance frequency is needed, the curve of the three technologies moves away in the opposite direction from the optimum point.

4.5.3 Conclusion

For a bending stiffness near 210^4 N/m^2, the CTM is a good choice of technology . Indeed, it is extremely lightweight and compact, with a weight and a radius of respectively 1.6 kg and 5 cm. However, if a better stiffness is needed, the only solution is to increase the occupied surface on the clamped side, which leads to a bulky structure. For example, with a bending stiffness of 10^5 N/m^2, the structure weighs approximately 3.5 kg with a radius a bit more than 8 cm .

Concerning the Telescopic boom, it is also limited by a lower boundary for the thickness but the latter is less restrictive than the CTM one. This technology offers a very good bending stiffness, but the weight and the cumbersome is much higher than the CTM. Regarding the Articulated boom, it offers the best bending stiffness. Unlike the Telescopic boom and the CTM, the Articulated boom has an upper boundary for the radius. In fact, a large diameter is not suitable for the folding operation. Thus, this technology is often used with a small diameter and a high thickness, which gives a very good bending stiffness. But, this structure is the heaviest. For the resonance frequency, the gap between the technologies concerning the weight is reduced. However, as for the bending stiffness, a better resonance frequency with the CTM means a higher boom diameter, thus a cumbersome system. Whereas the Articulated and Telescopic boom give a less bulky and heavier structure.

It seems that CTM is, by far, a better solution than the two other technologies. Yet, this technology has an Achilles' heel. The structure can be subjected to local deformation due to internal stresses, that distort the cross-section, which leads to the collapse of the structure. This effect is not studied in this thesis. Moreover, when the length increases, the structure becomes less stiff. Thus, the Articulated and the Telescopic booms become a better solution.

Nevertheless, the assumption of a maximum length of 3 meter is taken, in which case the Collapsible mast is an attractive solution as it is very lightweight. But, it is also too bulky for a good stiffness (above 10^5 N/m^2), which is needed to have a good stability and accuracy after deployment. If a technology does not reach a requirement, it should not be ruled out directly. In fact, some drawbacks can be compensated, as for example, the bending stiffness for the CTM can be increased by using several booms synchronously or by adding a mechanism to stiffen the structure.

At last, the CTM is chosen, its low weight offers a significant potential to make a less expensive and more compact deployable boom. The next step will be to check a configuration with several deployable booms and to confirm if this technology is suitable for small astrophysics mission.

Chapter 5

Pre-design

In this section, the pre-design of a deployable system with several Collapsible Tube Mast is constructed. This is a very simple design as the aim is to compare this system properties with the single boom one. To do that, the static analysis and the modal analysis are carried out for a similar load case as for the single boom. Finally, the results are compared.

5.1 Configuration

The first step is to decide on the number of CTM that will be used for the deployable system. Three booms seem to be a good choice. Indeed, two masts increase the stiffness of the system, but, there is still a lack of stability in the rotation and this drawback can be compensated by an additional mast. Moreover, adding a fourth boom will move away the system from the hyperstaticity configuration and the structure will becomes more complex. Therefore, a structure with 3 Collapsible masts is chosen.

Concerning the positioning, the figure 5.1 illustrates the three different possibilities that can be conceivable. The first one is when three booms are aligned, it increases the bending stiffness on the y-axis at the expense of the x-axis. Then, in order to improve the stiffness in the x-axis, the central boom can be moved upwards. Finally, the last configuration allows to increase the stiffness better in both directions. Tha is why it is selected. Regarding the orientation, the axis with the larger diameter is tangent to the circle of radius R, as it can be seen in Figure 5.2. In fact, with this configuration the torsional stiffness is the best.

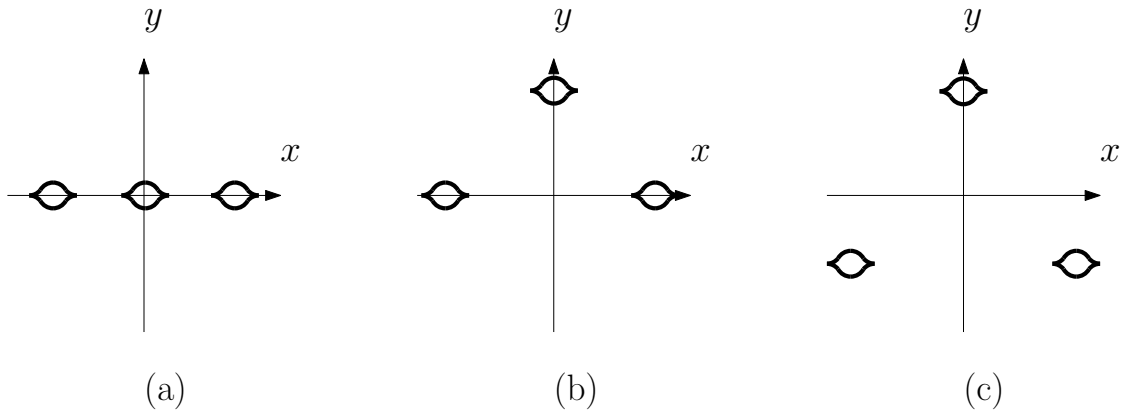

Figure 5.1: Positioning of the three Collapsible Tube Mast.

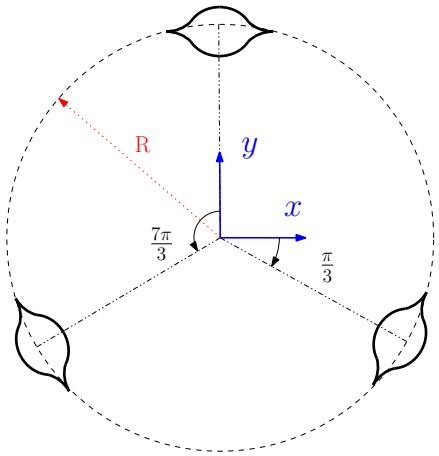

Figure 5.2: Orientation and placement of the three Collapsible Tube Masts.

Now, the boundary conditions are discussed. Like the single booms, the system is clamped at the satellite side. However, similar boundary condition as the single boom at the payload side can not be taken, since it will lead to a structure that will be 12 times hyperstatic. Indeed, the hyperstaticity is avoided as it has several drawbacks as follows. A hyperstatic structure needs a high accuracy in the manufacturing and in the assembling. An external perturbation can induce stresses in the structure as to thermal variation. Moreover, any geometric difference from the ideal geometry will cause significant internal stresses. As a result, it is better to consider an isostatic structure or, at least, try to have the smallest hyperstaticity degree.

The spherical joint and the planar joint are the two lower pair joints that cancel the less degree of freedom. The spherical joint is chosen to connect each mast to the

telescope platform. The system is thus 3 times hyperstatic. The behaviour of the spherical joint is not studied in this thesis.

5.2 Static analysis

In this subsection, the static analysis is conducted with the purpose of comparing the stiffness and the weight of this CTM system with the single boom structures.

Given that the structure is hyperstatic, a different method is used in order to compute the final deformation and thus the bending stiffness. The system is decomposed into two parts, on one side the 3 Collapsible Tube Masts and on the other side the payload platform that is illustrated by the simplified model presented in Figure 5.3. The geometric and material parameters of the 3 CTM are identical to the CTM studied in the previous chapter. The following assumptions are taken, the payload platform is considered as a rigid body. Indeed, the stiffness of the platform in compression and traction in the xy plane are considerably higher than the bending stiffness of the booms. Then, the centre of gravity of the Telescope-platform system is considered to be at a distance "d" from the end of the booms.

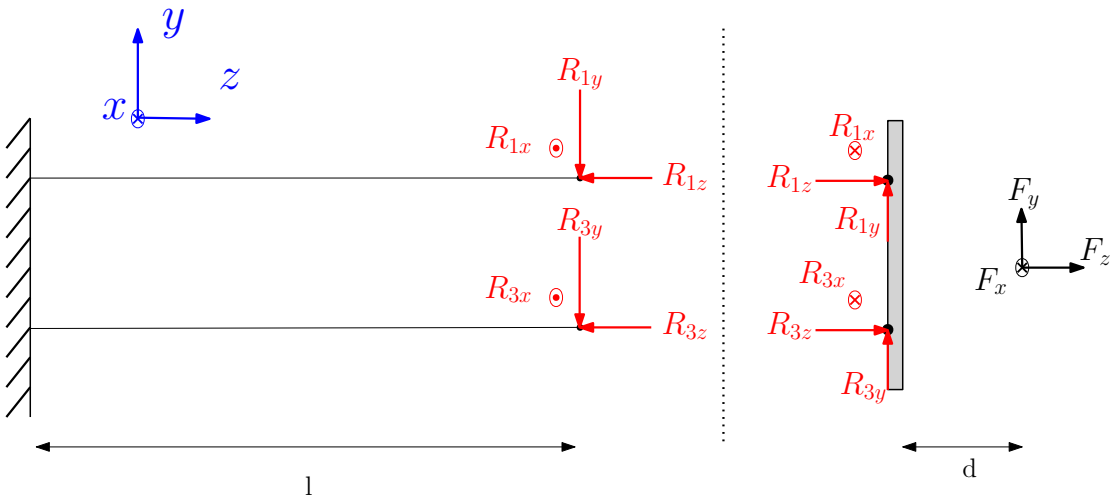

Figure 5.3: Simplified model of the system in the y-z plane.

First, the 6 equations of equilibrium are defined by using the simplified model of the payload platform in Figure 5.4.

$$R_{1x} + R_{2x} + R_{3x} + F_x = 0 \tag{5.1}$$

$$R_{1y} + R_{2y} + R_{3y} + F_y = 0 \tag{5.2}$$

$$R_{1z} + R_{2z} + R_{3z} + F_z = 0 \tag{5.3}$$

$$RR_{1z} - \frac{R}{2}R_{2z} - \frac{R}{2}R_{3z} + d\left(R_{1y} + R_{2y} + R_{3y}\right) = 0 \tag{5.4}$$

$$\frac{\sqrt{3}R}{2}R_{3z} - \frac{\sqrt{3}R}{2}R_{2z} - d\left(R_{1x} + R_{2x} + R_{3x}\right) = 0 \tag{5.5}$$

$$-RR_{1x} + \frac{R}{2}\left(R_{3x} + R_{2x}\right) + \frac{\sqrt{3}R}{2}\left(R_{2y} - R_{3y}\right) = 0 \tag{5.6}$$

where :
- R_{ij} is the reaction force at the end of the Collapsible Tube Mast i in the $j - axis$
- R is the distance between the centre of the platform and the different masts in the x-y plane.
- F_j represents the applied load due to the angular acceleration of the satellite in the $j - axis$.

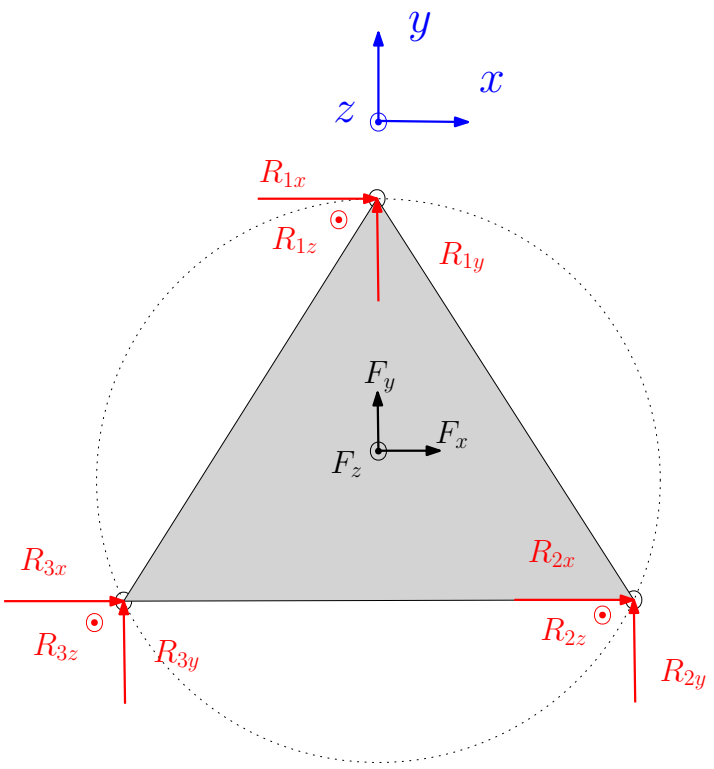

Figure 5.4: Simplified model of the platform in the x-y plane.

As the system is hyperstatic, the static equations are not sufficient to determine all the constraints. Thanks to the assumption of rigid body platform, 3 equations representing the compatibility between the connection points can be determined. In effect, the distance between the three connection points, with the platform, remains unchanged, which is defined as following

$$\left(v_{1x} - v_{2x} - \frac{\sqrt{3}R}{2}\right)^2 + \left(v_{1y} - v_{2y} + \frac{\sqrt{3}R}{2}\right)^2 + (v_{1z} - v_{2z})^2 = 0 \tag{5.7}$$

$$\left(v_{1x} - v_{3x} + \frac{\sqrt{3}R}{2}\right)^2 + \left(v_{1y} - v_{3y} + \frac{\sqrt{3}R}{2}\right)^2 + (v_{1z} - v_{3z})^2 = 0 \tag{5.8}$$

$$\left(v_{2x} - v_{3x} + \sqrt{3}R\right)^2 + (v_{2y} - v_{3y})^2 + (v_{2z} - v_{3z})^2 = 0 \tag{5.9}$$

where :
- v_{ij} is the deformation of the Collapsible Tube Mast i along j-axis.

The assumption of a rigid body platform entails a similar deformation of the 3 booms. These deformations can be computed thanks to the Euler-Bernoulli equation 4.16. The system of 9 equations and 9 unknowns is non linear, thus it can not be solved easily. The system of equations is resolved by using *Gradient descent*. Finally, the 6 reaction forces are computed by applying successively an angular acceleration along x-axis and y-axis. The values of these accelerations are the same values as the one determined in the "Load case" section, being 0.01 rad/s^2. The parameters R and d are arbitrarily chosen about respectively 0.35 m and 0.1 m.

Now, the single Collapsible Tube Mast structure and the system of CTM are compared. The bending stiffness in both direction are analysed in function of the radius and the weight. In fact, as the radius represents the same parameter with these structures, the latter can be used as comparison point.

Figure 5.5 illustrates the bending stiffness of 10^5 N/m^2 along y-axis in function of weight and radius. The curve of the Collapsible system is moved closer to the optimum point, as expected. Thus, the system is more lightweight. The latter also allows to use booms with smaller diameters. Moreover, the gap between the CTM and the Collapsible system enhances for a higher value of stiffness, as shows in Figure 5.6. This system can be further improved in order to use a more compact and a more lightweight system.

An important remark has to be made, the radius R of the circle containing the 3 Collapsible masts has no influence on the reaction forces in the transverse direction of the

booms. Therefore, it does not impact the bending stiffness of the structure. However, the radius has an affect on the axial deformation but the latter is not studied in this thesis.

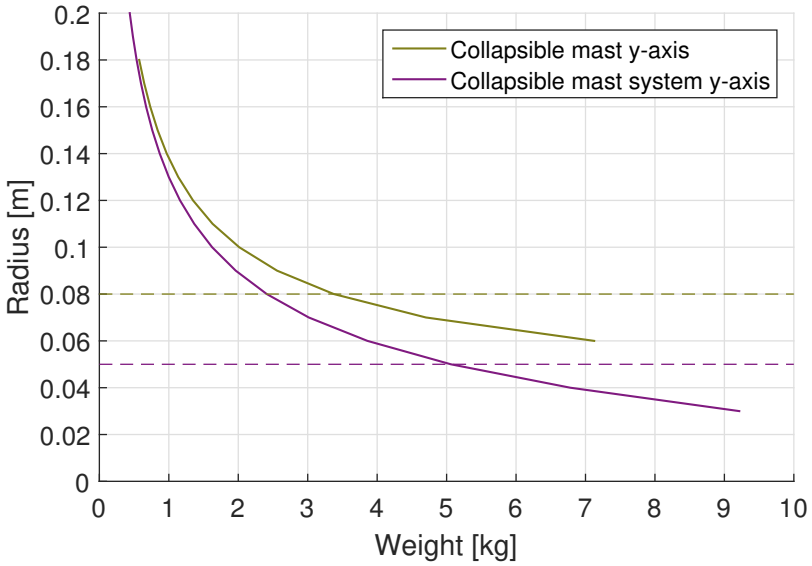

Figure 5.5: Boom radius in function of weight for the bending stiffness 10^5 N/m^2 of the y-axis of the Collapsible Tube Mast and of the Collapsible system.

5.2.1 Modal analysis

First, the modelling of the Collapsible system is carried out. This is performed, as explained in the previous chapter. Then, the computation of the eigen frequencies are done and the resonance frequency of a single Collapsible mast and the Collapsible mast system are compared.

Figure 5.7 illustrates the Collapsible system which is discretised into finit element. In this example Ndiv is equal to 10. the different elements are described by the different colours elements, while the black circle represents the main nodes of the system.

Figure 5.8 illustrates the resonance frequency of 10 Hz in function of the weight and the radius for the Collapsible Tube Mast and the Collapsible system. It can be seen that there is a great improvement. The Collapsible system allows to have a more compact and more lightweight system.

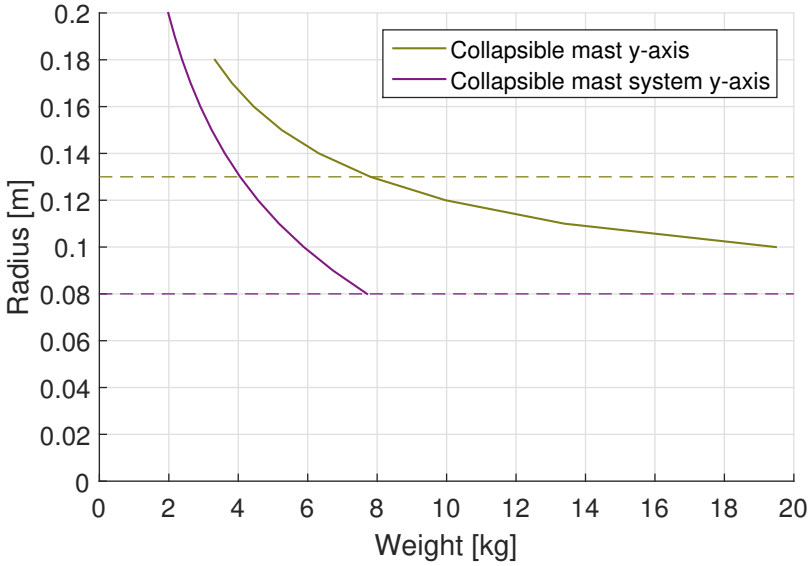

Figure 5.6: Boom radius in function of weight for the bending stiffness 5 10^5 N/m^2 of the y-axis of the Collapsible Tube Mast and of the Collapsible system.

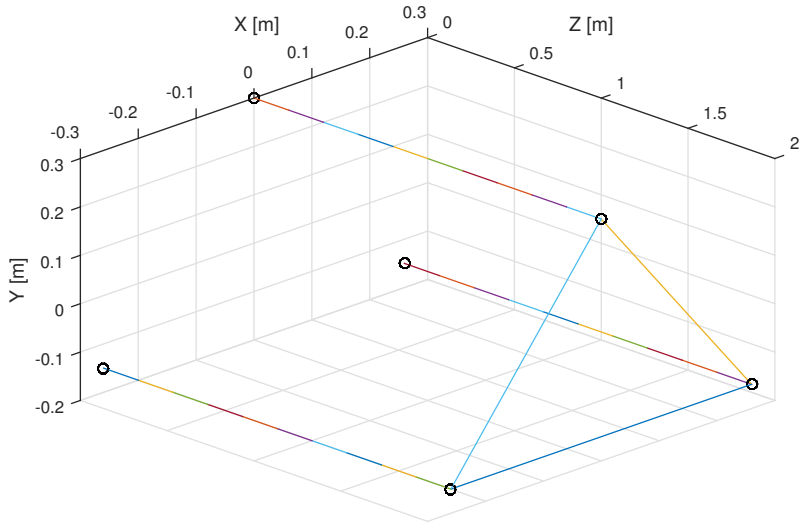

Figure 5.7: Discretization model of the Collapsible system.

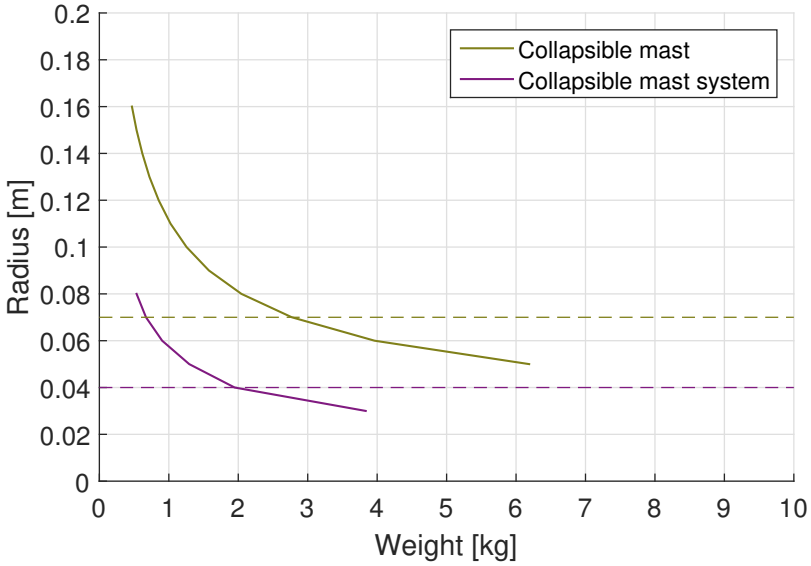

Figure 5.8: Boom radius in function of weight for a resonance frequency of 10 Hz of the Collapsible Tube Mast and of the Collapsible system.

5.3 Conclusion

By using several Collapsible Tube Masts, it is possible to obtain a system with better performances while decreasing its weight. However, the number of booms increases and thus the occupied area on the satellite side at the same time. But, it also allows to decreases the diameter of the different masts. Therefore, the retractable and deployable mechanism is also smaller, so it takes less space within the satellite.

The bending stiffness of the Collapsible system allows to obtain a deflection less than $1\mu m$ for a structure that weighs less than 10 kg, with geometric and material properties describe in the previous chapter.

This small pre-design proves that several Collapsible Tube Masts can be used together in order to increase the post-deployment accuracy, the compactness and the weight of the system. By optimising this design, a very compact and lightweight structure can be obtained and the latter can be used for astrophysics application.

Chapter 6

Further work

Before the concluding, it is interesting to mentioned the further study that can be carried out in order to continue the development.

Firstly, the CTM is made of thin strips, they can be subjected to local deformations due to thermal effects or to internal stresses. This deformation leads to the collapse of the structure. In a further work, it is important to analyse this in details.

Then, the deployable/retractable mechanism is not studied. In fact, this is a complex mechanism that is composed of different parts such as the storage reel, the different rollers that perform the flattening of the strip, the support Collar etc. All of this depends on the mast dimensions. Once this mechanism is defined, it will allow to accurately determine the storage volume, the power needed to fold/unfold the structure and the deployment accuracy.

The assembly between the collapsible masts and the payload platform is assumed to be performed with spherical joints. However, this type of joint have some disadvantages as bringing play between the masts and the payload platform. This part is extremely important and a careful analysis should be undertaken.

Another study that needs to be carried out is about the thermal effects. In fact, spacecraft are subjected to significant thermal gradients or the shadowing of a part of the system that induces thermal deformation. A work should be done to verify if the structure withstands this perturbations.

Afterwards, a work on the dynamic response of the structure can be conducted. In this thesis, the eigen frequencies are determined. To go further, one can determine the damping and then, analyse the forced response. The damping of a structure can be enhanced by using a passive damping method or an active damping technology. The latter consists in applying an equal and opposite force to eliminate the undesired

vibration.

Finally, the requirement about the deployment accuracy and the post-deployment accuracy is assumed to be 40nm. This requirement can not be reached with only one booms structure. In effect, one or several stages of active structure can be considered. This control technology is widely used in the field of precision mechanics. An alternative is the use of optical delay line that is also generally used in this field.

Chapter 7

Conclusion

The objective of this thesis is the development of a deployable structure for a small mission of PROBA type in order to provide a baseline for a space interferometric instrument.

The first part was related to the sate of the art, in which the main applications that use the deployable structure are presented. It follows by the description of the different technologies of deployable arm currently available with their advantages and drawbacks.

Then, a small introduction on the space interferometry is presented in order to define the problem and to determine the requirements needed for the space based observatory. The specifications associated to the mission are defined.

Afterwards, a first technology selection is carried out. To do so, the different technologies are compared on the basis of other researchers' work and experimental data available. This enables to figure out which structures are intrinsically not suitable for an astrophysics application, which ones do not correspond to the specifications related to this mission and which ones are potentially well suited.

From this selection, three structures come out: the Telescopic boom, the Articulated boom and the Thin-walled deployable boom. A first pre-design is performed and especially the Collapsible Tube Mast is characterised as it does not have a standard shape.

After that, the static analysis is conducted on the three technologies. The aim is to compare which technology satisfies the best the requirements concerning the weight of the arm, the volume and the post-deployment accuracy which is related to the stiffness of the structure and particularly to the bending stiffness

Next, Eigen frequencies are determined. To do so, a finite element model is performed in MATLAB by the use of "3D beam finite elements". This enables to model the three technologies and to find out their eigen frequencies. The latter are compared to the same requirements as the bending stiffness.

The analyses result in the selection of the Collapsible Tube Mast that is considered the most appropriate structure for a small deployable boom of 1 to 3 meters.

After that, a pre-design of a system composed of three Collapsible masts is carried out in order to obtain a better deployable mechanism. To this end, a static analysis is performed in order to verify the improvement of the deployable structure that fulfills better the requirements, particularly the reduction of the bulk.

Finally, an eigenfrequency study is done and the latter shows very clearly the improvements of the structure.

At last, all these analyses confirm that a deployable structure for small astrophysics missions is feasible with the Collapsible system. But this work does not cover all the aspects of this complex structure. Additional work is needed for the good development of the deployable structure.

Appendices

Appendix A

Detailed static analysis developments

This appendix presents the development of the calculation of the moments and the forces acting within the first, second and third segments by using free body diagrams. At the end, the solution of the equation 4.17 for the four segments is also displayed.

The third segment

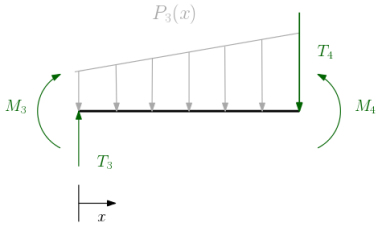

with :

-$P_3(x) = S_3.\rho.\ddot{\alpha}.\left(x + \frac{l}{2}\right)$

Figure A.1: Free body diagrams of the third section of the boom.

$$T_3 = \int_0^{l/4} P_3(x)dx + T_4 = S_3\rho\ddot{\alpha}.\frac{5l^2}{32} + M_{load}l\ddot{\alpha} + S_4\rho\ddot{\alpha}\frac{7l^2}{32}$$

$$M_3 = M_4 - \int_0^{l/4} P_3(x)xdx - \frac{l}{4}\left(M_{load}l\ddot{\alpha} + S_4\rho\ddot{\alpha}\frac{7l^2}{32}\right) = -M_{load}\frac{l^2\ddot{\alpha}}{2} - S_4\rho\ddot{\alpha}\frac{l^3}{2} - S_3\rho\ddot{\alpha}\frac{l^3}{48}$$

Moments and forces acting within the third boom segment are given by

$$T_3(x) = S_3\rho\ddot{\alpha}\left(\frac{5l^2}{32} - \frac{x^2}{2} - \frac{lx}{2}\right) + M_{load}l\ddot{\alpha} + S_4\rho\ddot{\alpha}\frac{7l^2}{32}$$
$$M_3(x) = M_{load}\ddot{\alpha}\left(lx - \frac{l^2}{2}\right) + S_4\rho\ddot{\alpha}\left(\frac{7l^2}{32} - \frac{l^3}{12}\right) + S_3\rho\ddot{\alpha}\left(\frac{5l^2}{32} - \frac{l^3}{48} - \frac{x^3}{3} - \frac{lx^2}{4}\right)$$

The second segment

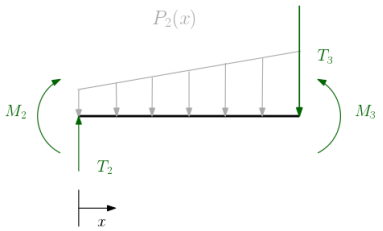

with :

-$P_3(x) = S_3.\rho.\ddot{\alpha}.\left(x + \frac{l}{4}\right)$

Figure A.2: Free body diagrams of the second section of the boom.

$$T_2 = \int_0^{l/4} P_2(x) + T_3 = M_{load}l\ddot{\alpha} + S_4\rho\ddot{\alpha}\frac{7l^2}{32} + S_3\rho\ddot{\alpha}\frac{5l^2}{32} + S_2\rho\ddot{\alpha}\frac{3l^2}{32}$$
$$M_2 = M_3 - \int_0^{l/4} P_2(x)xdx - T_3\frac{l}{4} = -M_{load}\frac{3l^2\ddot{\alpha}}{4} - \frac{53}{384}S_4\rho\ddot{\alpha}l^3 - \frac{47}{384}S_3\rho\ddot{\alpha}l^3 - \frac{5}{384}S_2\rho\ddot{\alpha}l^3$$

Given that the moments and forces in the second boom segment can be determined

$$T_2(x) = M_{load}l\ddot{\alpha} + S_4\rho\ddot{\alpha}\frac{7l^2}{32} + S_3\rho\ddot{\alpha}\frac{5l^2}{32} + S_2\rho\ddot{\alpha}\left(\frac{3l^2}{32} - \frac{x^2}{2} - \frac{lx}{4}\right)$$
$$M_2(x) = M_{load}\ddot{\alpha}\left(-\frac{3l^2}{4} + xl\right) + S_4\rho\ddot{\alpha}\left(-\frac{53l^3}{384} + \frac{7l^2x}{32}\right) + S_3\rho\ddot{\alpha}\left(-\frac{5l^3}{384} + \frac{5l^2x}{32}\right)$$
$$+ S_2\rho\ddot{\alpha}\left(-\frac{5l^3}{384} + \frac{3l^2x}{32}\right)$$

The first segment

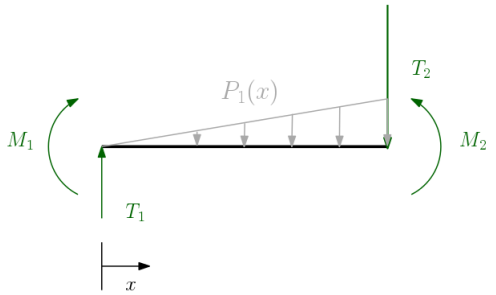

with :

-$P_3(x) = S_3.\rho.\ddot{\alpha}.x$

Figure A.3: Free body diagrams of the first section of the boom.

$$T_1 = \int_0^{l/4} P_1(x)dx + T_2 = M_{load}l\ddot{\alpha} + S_4\rho\ddot{\alpha}\frac{7l^2}{32} + S_3\rho\ddot{\alpha}\frac{5l^2}{32} + S_2\rho\ddot{\alpha}\frac{3l^2}{32} + S_1\rho\ddot{\alpha}\frac{l^2}{32}$$

$$M_1 = M_2 - \int_0^{x} P_1(x)xdx - T_2x = -M_{load}l^2\ddot{\alpha} - \frac{37}{192}S_4\rho\ddot{\alpha}l^3 - \frac{5}{96}S_3\rho\ddot{\alpha}l^3 - \frac{7}{192}S_2\rho\ddot{\alpha}l^3 - S_1\rho\ddot{\alpha}\frac{l^3}{192}$$

The last internal moments and forces can be obtained by

$$T1_(x) = M_{load}l\ddot{\alpha} + S_4\rho\ddot{\alpha}\frac{7l^2}{32} + S_3\rho\ddot{\alpha}\frac{5l^2}{32} + S_2\rho\ddot{\alpha}\frac{3l^2}{32} + S_1\rho\ddot{\alpha}\left(\frac{l^2}{32} - \frac{x^2}{2}\right)$$

$$M_1(x) = M_{load}\ddot{\alpha}\left(-l^2 + xl\right) + S_4\rho\ddot{\alpha}\left(-\frac{37l^3}{192} + \frac{7xl^2}{32}\right) + S_3\rho\ddot{\alpha}\left(\frac{-5l^3}{96} + \frac{5l^2x}{32}\right)$$
$$+ S_2\rho\ddot{\alpha}\left(-\frac{7l^3}{192} + \frac{3l^2x}{32}\right) + S_1\rho\ddot{\alpha}\left(-\frac{l^3}{192} + \frac{l^2x}{32} - \frac{x^3}{3}\right)$$

Appendix B

Elementary stiffness matrix in local axes

$$\boldsymbol{K}_{el} = \begin{bmatrix}
\frac{EA}{l} & & & & & & & & & & & \\
0 & \frac{12EI_z}{l^3} & & & & & & & & & & \\
0 & 0 & \frac{12EI_y}{l^3} & & & & & & & & & \\
0 & 0 & 0 & \frac{GJ_x}{l} & & & & & & & & \\
0 & 0 & \frac{-6EI_y}{l^2} & 0 & \frac{4EI_y}{l} & & & & & & & \\
0 & \frac{6EI_z}{l^2} & 0 & 0 & 0 & \frac{4EI_z}{l} & & & & & & \\
\frac{-EA}{l} & 0 & 0 & 0 & 0 & 0 & \frac{EA}{l} & & & & & \\
0 & \frac{-12EI_z}{l^3} & 0 & 0 & 0 & \frac{-6EI_z}{l^2} & 0 & \frac{12EI_z}{l^3} & & & & \\
0 & 0 & \frac{-12EI_y}{l^3} & 0 & \frac{6EI_y}{l^2} & 0 & 0 & 0 & \frac{12EI_y}{l^3} & & & \\
0 & 0 & 0 & \frac{-GJ_x}{l} & 0 & 0 & 0 & 0 & 0 & \frac{GJ_x}{l} & & \\
0 & 0 & \frac{-6EI_y}{l^2} & 0 & \frac{2EI_y}{l} & 0 & 0 & 0 & \frac{6EI_y}{l^2} & 0 & \frac{4EI_y}{l} & \\
0 & \frac{6EI_z}{l^2} & 0 & 0 & 0 & \frac{2EI_z}{l} & 0 & \frac{-6EI_z}{l^2} & 0 & 0 & 0 & \frac{4EI_z}{l}
\end{bmatrix}$$

SYM

- A : Area of the section
- r : The radius of gyration of the cross section, $r = \sqrt{\frac{I_y + I_z}{A}}$
- I_y : Second moment of area in the y axis
- I_z : Second moment of area in the z axis
- J_x : Torsional constant of the cross section
- E : The Young's Modulus
- ρ : The density of the material
- G : The shear modulus
- l : The length of an element

Elementary mass matrix in local axes

$$M_{el} = \rho A l \begin{bmatrix} \frac{1}{3} & & & & & & & & & & & \\ 0 & \frac{13}{35} & & & & & & & & & & \\ 0 & 0 & \frac{13}{35} & & & & & & & & & \\ 0 & 0 & 0 & \frac{r^2}{3} & & & & & & & & \\ 0 & 0 & \frac{-11l}{210} & 0 & \frac{l^2}{105} & & & & & & & \\ 0 & \frac{11l}{210} & 0 & 0 & 0 & \frac{l^2}{105} & & & & & & \\ \frac{1}{6} & 0 & 0 & 0 & 0 & 0 & \frac{1}{3} & & & & & \\ 0 & \frac{9}{70} & 0 & 0 & 0 & \frac{13l}{420} & 0 & \frac{13}{35} & & & & \\ 0 & 0 & \frac{9}{70} & 0 & \frac{-13l}{420} & 0 & 0 & 0 & \frac{13}{35} & & & \\ 0 & 0 & 0 & \frac{r^2}{6} & 0 & 0 & 0 & 0 & 0 & \frac{r^2}{3} & & \\ 0 & 0 & \frac{13l}{420} & 0 & \frac{-l^2}{140} & 0 & 0 & 0 & \frac{11l}{210} & 0 & \frac{l^2}{105} & \\ 0 & \frac{-13l}{420} & 0 & 0 & 0 & \frac{-l^2}{140} & 0 & \frac{-11l}{210} & 0 & 0 & 0 & \frac{l^2}{105} \end{bmatrix} \quad SYM$$

Bibliography

[1] Dawn spacecraft mission overview – spacecraft satellites. http://spaceflight101.com/spacecraft/dawn-spacecraft-mission-overview/.

[2] Inflatable solar array technology packs incredible power in small pack. https://www.nasa.gov/centers/marshall/news/news/releases/2014/14-112.html.

[3] Northrop grumman astro aerospace's astromesh for NASA jpl's smap. https://www.northropgrumman.com/BusinessVentures/AstroAerospace/Pages/SMAP.aspx.

[4] Iae-eoportal directory-satellite missions. https://www.northropgrumman.com/BusinessVentures/AstroAerospace/Pages/SMAP.aspx.

[5] S.D. Guest and S. Pellegrino. A new concept for solid surface deployable antennas. *Pergamon*, pages 103–113, 3 1995. Cambridge University Engineering Department.

[6] Prism-eoportal directory-satellite missions. https://directory.eoportal.org/web/eoportal/satellite-missions/p/prism.

[7] Gabriele Porrometo. L'après hubble:le nouveau télescope spatial de la Nasa est terminé-tech-numerama. https://www.numerama.com/tech/207313-lapres-hubble-le-nouveau-telescope-spatial-de-la-nasa-est-termine.html.

[8] Inflatable boom of nasa, johnson space center. https://www.nasa.gov/mission_pages/station/research/experiments/RIGEX2.jpg.

[9] F. Jensen and S. Pellegrino. Arm development review of existing technologies. 2001.

[10] M.W. Thomson. Deployable and retractable telescoping tubular structure development. 1994.

[11] Oxford space systems. https://oxford.space/#s-technology.

[12] Srtm-eoportal directory-satellite missions. https://directory.eoportal.org/web/eoportal/satellite-missions/s/srtm.

[13] A study of the axiom mission: boom design. http://www.mssl.ucl.ac.uk/~gbr/kirill/booms.html.

[14] Alex Brinkmeyer, Sergio Pellegrino, and Paul M. Weaver. Effects of long-term stowage on the deployment of bistable tape springs. *Journal of Applied Mechanics - The American Society of Mechanical*, 11 2015.

[15] F. Hakkak and S. Khoddam. On calculation of preliminary design parameters for lenticular booms. *Journal of Aerospace Engineering*, 3 2007.

[16] W. Keith Belvin, Marco Straubel, W. Keats Wilkie, Martin E. Zander, Juan M. Fernandez, and Martin F. Hillebrandt. Advanced deployable structural systems for small satellites. *NASA Technical Reports Server*, 9 2016. NASA Langley Research Center; Hampton, VA, United States.

[17] How hubble got its wings. http://www.esa.int/Our_Activities/Space_Engineering_Technology/How_Hubble_got_its_wings.

[18] Spx-8 spacex dragon spacecraft grappled by ssrms - NASA image and video library. https://images.nasa.gov/details-iss047e050978.html.

[19] Articulated deployment systems - airbus defence space dutch technology. https://www.airbusdefenceandspacenetherlands.nl/products/articulated-deployment-systems/.

[20] Antenna arraying - deep space network. https://deepspace.jpl.nasa.gov/about/complexes/antenna-arraying/.

[21] Aerial view of the vlti with tunnels superimposed. http://www.eso.org/public/images/eso0111f/.

[22] L.Puig, A.Barton, and N.Rando. A review on large deployable structures for astrophysics missions. *Elsevier*, 2010.

[23] Jwst-eoportal directory-satellite missions. https://directory.eoportal.org/web/eoportal/satellite-missions/j/jwst.

[24] Mark Schenk, Andrew D. Viquerat, Keith A. Seffen, and Simon D. Guest. Review of inflatable booms for deployable space structures: Packing and rigidization. *Journal of Spacecraft and Rockets*, 2014.

[25] Jason G. Budinoff, David Leisawitz, Buddy Taylor, and Drew Jones. Mechanical design of the space infrared interferometric telescope (spirit).

[26] Nasa - canadarm2 and the mobile servicing system. https://www.nasa.gov/mission_pages/station/structure/elements/mss.html.

[27] Very large telescope. http://www.eso.org/public/teles-instr/paranal-observatory/vlt/.

[28] D.E. Koelle and R. Janovsky. Development and transportation costs of space launch systems. *DGLR/CEAS - European Air and Space Conference*, 2007.

[29] Esa science technology: Far infrared interferometer. `http://sci.esa.int/trs/40090-far-infrared-interferometer/`.

[30] Esa science technology: Advanced telescope for high energy astrophysics. `http://sci.esa.int/ixo/48729-about-athena/`.

[31] ZhongYi, Chu, YiAn, and Lei. Design theory and dynamic analysis of a deployable boom. *Journal Mechanism and Machine Theory - Elsevier*, 10 2013.

[32] Shahin Khoddam and Feras Hakak. On calculation of preliminary design parameters for lenticular boom. *Journal of Aerospace Engineering*, 3 2007.

[33] Michel Géraldin and Daniel J. Rixen. *Mechanical Vibrations*. 2015.